The Plant Cell, Vol. 27: 1297–1315, April 2015, www.plantcell.org

Salt-Induced Remodeling of Spatially Restricted Clathrin-Independent Endocytic Pathways in Arabidopsis Root

Anirban Baral,[a] Niloufer G. Irani,[a,1] Masaru Fujimoto,[b,c] Akihiko Nakano,[c,d] Satyajit Mayor,[a,2] and M.K. Mathew[a,2]

[a] National Centre for Biological Sciences, TIFR, Bangalore, Karnataka 560065, India
[b] Laboratory of Plant Molecular Genetics, Graduate School of Agricultural and Life Sciences, University of Tokyo, Bunkyo-Ku, Tokyo 113-8657, Japan
[c] Department of Biological Sciences, Graduate School of Science, University of Tokyo, Bunkyo-Ku, Tokyo 113-0033, Japan
[d] Live Cell Molecular Imaging Research Team, RIKEN Center for Advanced Photonics, Wako, Saitama 351-0198, Japan

ORCID IDs: 0000-0003-3252-4493 (N.G.I.); 0000-0001-9842-6963 (S.M.); 0000-0002-5932-3598 (M.K.M.)

Endocytosis is a ubiquitous cellular process that is characterized well in animal cells in culture but poorly across intact, functioning tissue. Here, we analyze endocytosis throughout the *Arabidopsis thaliana* root using three classes of probes: a lipophilic dye, tagged transmembrane proteins, and a lipid-anchored protein. We observe a stratified distribution of endocytic processes. A clathrin-dependent endocytic pathway that internalizes transmembrane proteins functions in all cell layers, while a sterol-dependent, clathrin-independent pathway that takes up lipid and lipid-anchored proteins but not transmembrane proteins is restricted to the epidermal layer. Saline stress induces a third pathway that is clathrin-independent, nondiscriminatory in its choice of cargo, and operates across all layers of the root. Concomitantly, small acidic compartments in inner cell layers expand to form larger vacuole-like structures. Plants lacking function of the Rab-GEF (guanine nucleotide exchange factor) VPS9a (vacuolar protein sorting 9A) neither induce the third endocytic pathway nor expand the vacuolar system in response to salt stress. The plants are also hypersensitive to salt. Thus, saline stress reconfigures clathrin-independent endocytosis and remodels endomembrane systems, forming large vacuoles in the inner cell layers, both processes correlated by the requirement of VPS9a activity.

INTRODUCTION

Multiple pathways of endocytosis have been identified in animal systems that vary in terms of the molecular constituents involved and also by the type of cargo that is internalized (Doherty and McMahon, 2009). Most studies have utilized isolated cells in culture, apart from some recent studies in developing embryos of *Caenorhabditis elegans* and *Drosophila melanogaster*. The latter studies raise the possibility that endocytic processes may be differentially regulated across different cell lineages (Andrews and Ahringer, 2007; Mateus et al., 2011). Endocytic mechanisms may thus be expected to vary across cell types in an intact, functional tissue and, moreover, may be subject to differential regulation in response to diverse physiological conditions. The best-characterized endocytic mechanism is clathrin-mediated endocytosis (Taylor et al., 2011). However, pathways independent of clathrin are also reported to operate in animal cells, including one that mediates the uptake of glycosyl phosphatidyl inositol (GPI)-anchored proteins in GPI-anchored protein-enriched early endocytic compartments via the formation of clathrin-independent carriers (Sabharanjak et al., 2002).

Although the operation and physiological relevance of endocytosis have been demonstrated unequivocally in plants, the molecular components participating in the process are less well characterized than in animal systems. Simple, well-defined tissue organization makes the *Arabidopsis thaliana* root an ideal system to study endocytic events across different cell layers. Most extant studies, however, have been confined to the epidermal layer at the surface of the root. These studies, together with others on cultured plant cells in suspension, have revealed the operation of at least two endocytic mechanisms. All transmembrane proteins studied so far have been shown to follow the clathrin-dependent uptake pathway, which operates in all cell layers of the Arabidopsis root (Robert et al., 2010; Kitakura et al., 2011), but information on other pathways is scarce. Clathrin-independent pathways have been implicated in studies of tobacco (*Nicotiana tabacum*) cells grown in suspension culture (Onelli et al., 2008) and in epidermal cells of Arabidopsis root (X. Li et al., 2011; R. Li et al., 2012), but neither of these pathways has been characterized with respect to the identity of cargo handled or the range of operation beyond the epidermis. Furthermore, the functions of these pathways have not been investigated in any metazoan system; therefore, the study of the role of this pathway in plants would represent an important step in this direction (Mayor et al., 2014).

Here, we have exploited the optical transparency and physical accessibility of young Arabidopsis roots to explore the full panoply of endocytic mechanisms in different cell layers. We have probed uptake mechanisms utilizing a range of probes and varied physiological conditions. GPI-anchored proteins resemble

[1] Current address: Department of Plant Sciences, University of Oxford, Oxford OX13RB, UK.
[2] Address correspondence to mayor@ncbs.res.in or mathew@ncbs.res.in. The author responsible for distribution of materials integral to the findings presented in this article in accordance with the policy described in the Instructions for Authors (www.plantcell.org) is M.K. Mathew (mathew@ncbs.res.in).
www.plantcell.org/cgi/doi/10.1105/tpc.15.00154

glycolipids with large protein head groups. Unsurprisingly, in animal cells, they follow an uptake pathway distinct from transmembrane proteins with cytoplasmic tails that bear endocytic signals. Speculating that such proteins could utilize clathrin-independent pathways in plants as well, we attached a GPI anchor signal sequence (Eisenhaber et al., 2003) from the Arabidopsis GPI-anchored protein COBRA (Roudier et al., 2005) to the C terminus of a secretory version of green fluorescent protein (GFP)/mCherry. Along with GPI-tethered fluorescent proteins (GFP/mCherry-GPI), we monitored the endocytosis of the endocytic tracer dye FM4-64 (Bolte et al., 2004) as a reporter for bulk membrane uptake and utilized several transmembrane proteins as cargo for clathrin-dependent endocytosis. We have used these three sets of probes to explore endocytic mechanisms in Arabidopsis roots and tobacco BY-2 cells. Our study, spanning all cell layers of the intact tissue, establishes that clathrin-dependent endocytosis operates in all cell layers of the root, consistent with previous observations. By contrast, a clathrin-independent endocytic pathway operates in the epidermal cell layer but not in the internal layers of the Arabidopsis root tip. Finally, we report that salinity stress induces an additional clathrin-independent bulk-flow endocytic pathway in all cell layers of the Arabidopsis root that is critically dependent on the function of the Rab-GEF (guanine nucleotide exchange factor) VPS9a (Goh et al., 2007). This study thus establishes that multiple endocytic pathways operate within a stratified tissue and that these pathways are differentially regulated across cell types by physiologically relevant stimuli.

RESULTS

GPI-Anchored Proteins Are Endocytosed from the Plasma Membrane in Plant Cells

To monitor the intracellular distribution of GPI-anchored proteins, we observed Arabidopsis roots and tobacco BY-2 cells expressing the mCherry/GFP-GPI cassette from a cauliflower mosaic virus 35S promoter (Figure 1A). Fluorescence signal was detected at the cell periphery and intracellular vesicular structures (Figure 1B, left). Upon plasmolysis of root epidermal cells of GFP-GPI plants with 600 mM sucrose, GFP remained associated with the plasma membrane (PM) and not the cell wall or periplasmic space (Figure 1B, right).

PM localization of GFP-GPI was shown by surface immunostaining of unpermeabilized BY-2 protoplasts (Supplemental Figure 1A). This result also indicates that the GFP moiety faces the cell wall, as expected for an exofacial lipid-tethered protein. We verified that the GFP is indeed tethered to the PM by a GPI anchor using a Triton X-114 partitioning assay together with treatment with phosphatidylinositol-specific phospholipase C, an enzyme that specifically cleaves the GPI anchor (Roudier et al., 2005) (Supplemental Figure 1B).

To ascertain the nature of the cytoplasmic bodies in which GFP-GPI was observed, pulse-chase experiments were performed in BY-2 cells and Arabidopsis roots with the endocytic tracer dye FM4-64 (Bolte et al., 2004). After 10 min of chase, FM4-64-containing nascent endocytic vesicles colocalized with GFP-GPI in the vicinity of the PM in root epidermal cells (Figure 1C). After a longer chase period of 30 min, GFP-GPI vesicles almost completely colocalized with FM4-64 in BY-2 cells (Supplemental Figure 1C) as well as root epidermal cells. The endocytic character of GFP-GPI vesicles was further examined by treatment with the drug brefeldin A (BFA). BFA causes endosomal compartments and the endocytosed cargo within to clump into large intracellular aggregates termed BFA bodies (Geldner et al., 2001). Upon treatment with BFA, both in BY-2 cells and in Arabidopsis root, large aggregates, characteristic of BFA bodies, were formed that contained both GFP-GPI and FM4-64 (Figure 1D; Supplemental Figure 1D). A functional GFP fusion of the endogenous GPI-anchored protein SKU5 (Sedbrook et al., 2002) showed similar trafficking properties to GFP-GPI in Arabidopsis root (Supplemental Figures 2A and 2B).

Intracellular vesicles of GFP/mCherry-GPI partially colocalized with the endosomal markers (Ueda et al., 2001) ARA6-GFP (Pearson's coefficient, 0.51 $\pm$ 0.07; n = 74 cells) and ARA7-GFP in root epidermal cells and formed aggregates together when treated with BFA (Figures 1E and 1F; Supplemental Figures 1E and 1F). However, GFP-GPI punctae showed little colocalization with the Golgi marker SYP32-RFP (red fluorescent protein) (Uemura et al., 2004; Geldner et al., 2009) (Pearson's coefficient, 0.12 $\pm$ 0.05; n = 70 cells) (Supplemental Figure 1G). Upon BFA treatment, GFP-GPI aggregated in the center of the BFA bodies and was clearly separated from SYP-32-marked Golgi stacks that were arranged in the fringes (Supplemental Figure 1H). Such differential response to BFA has been used as a marker to distinguish the endosomal/*trans*-Golgi network (TGN) from Golgi bodies in Arabidopsis root cells (Geldner et al., 2009). Similar characteristics were observed in transiently transfected BY-2 cells/protoplasts with ARA6-GFP or the Golgi marker soybean (*Glycine max*) mannosidase-1-RFP (Nelson et al., 2007) (Supplemental Figures 1I to 1K).

To ascertain the endocytic uptake of GPI-anchored proteins from PM in living root tissue, we observed Arabidopsis root epidermal cells expressing mCherry-GPI and clathrin light chain (CLC)-GFP using variable-angle epifluorescence microscopy (VAEM), which allows imaging of events on or immediately beneath the PM (Konopka and Bednarek, 2008). Under VAEM, PM-localized mCherry-GPI appeared as dynamic and well-demarcated cortical-associated foci embedded within diffuse and weaker background fluorescence (Supplemental Movie 1). We found that this background fluorescence was quickly photobleached within the first few frames of acquisition, whereas the brighter punctate structures photobleach over a longer time scale, making it possible to track the formation and internalization of such foci over time (we have sorted images to ensure that we are not monitoring intracellular punctate structures and organelles such as TGNs; see Methods). Some mCherry-GPI foci colocalized with CLC-GFP foci, while others did not (dashed versus solid circles in Figure 1G; Supplemental Figure 3A). Analysis of 10 different dual-color mCherry-GPI/CLC-GFP VAEM images containing a total of 2801 mCherry-GPI foci revealed that 68.23% $\pm$ 3.86% of such foci colocalized with CLC-GFP (Supplemental Figure 3E). However, the remaining mCherry-GPI foci were devoid of CLC-GFP. To rule out the possibility that the observed colocalization between CLC-GFP

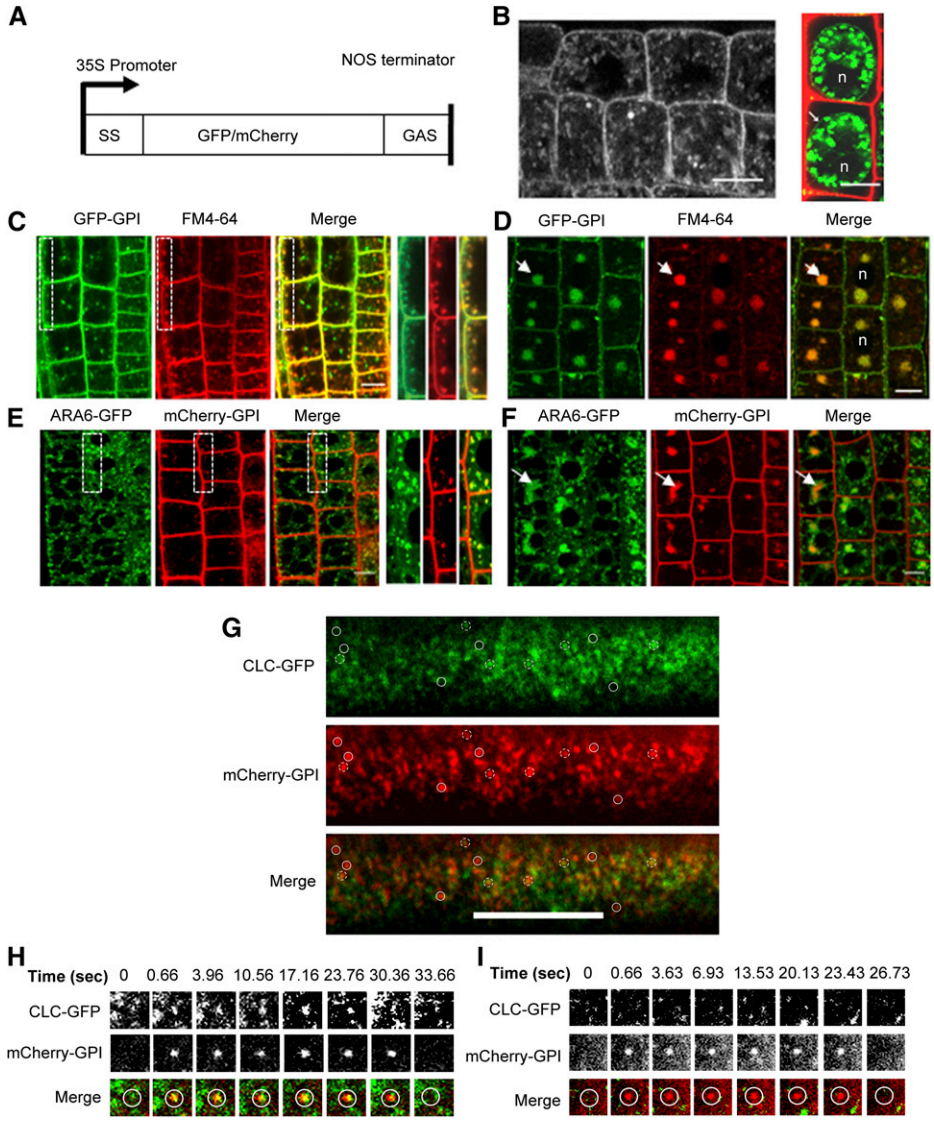

Figure 1. GPI-Anchored Proteins Are Endocytosed from the PM.

(A) Schematic representation of the GPI reporter cassette. SS, secretory signal sequence from Arabidopsis basic chitinase; GAS, GPI anchor signal sequence from At-*COBRA*.

(B) Arabidopsis root epidermal cells (left) expressing GFP-GPI. Plasmolysis of GFP-GPI roots with 600 mM sucrose (right) reveals that GFP-GPI is associated with the PM (white arrow) rather than the cell wall, which is stained with propidium iodide (red).

(C) GFP-GPI-expressing Arabidopsis roots pulsed with 5 μM FM4-64 for 5 min on ice, washed, and then chased for 10 min at room temperature. Enlarged images of the boxed areas are presented on the right.

(D) Arabidopsis root epidermal cells pulsed with FM4-64 for 5 min and then treated with 50 μm BFA for 1 h. White arrows mark a BFA body.

(E) Arabidopsis root epidermal cells expressing ARA6-GFP and mCherry-GPI. Enlarged versions of the boxed areas are shown on the right.

(F) ARA6-GFP- and mCherry-GPI-expressing Arabidopsis root treated with 50 μm BFA for 1 h. White arrows mark a BFA body.

(G) VAEM images of Arabidopsis root epidermal cells expressing GFP-CLC (green) and mCherry-GPI (red). Examples of mCherry-GPI foci colocalizing with and devoid of CLC-GFP are marked with dashed and solid white circles, respectively.

(H) and **(I)** Time-lapse snapshots from Supplemental Movies 2 and 3 showing clathrin-dependent **(H)** and independent **(I)** uptake of mCherry-GPI foci. n, nucleus. Bars = 10 μm.

and mCherry-GPI foci was due to random overlap, the red channel image from five different cells was rotated 180° with respect to the green channel (Delcroix et al., 2003; Konopka et al., 2008). The percentage of mCherry-GPI foci that colocalized with CLC-GFP foci in the rotated images (37.64% ± 5.03%) was significantly lower than that in the original image (67.52% ± 7.58%; n = 1058 foci, $P < 0.000001$). Pearson's coefficients for original and rotated images were 0.48 ± 0.12 and 0.0498 ± 0.09, respectively ($P < 0.0001$). The formation and internalization of both classes of mCherry-GFP foci could be observed under time-lapse imaging (300-ms exposure time; see Supplemental Movies 2 and 3 for clathrin-dependent and clathrin-independent uptake of mCherry-GPI, respectively). Sequences of images from these movies (Figures 1H and 1I) show the appearance and internalization of mCherry foci together with, as well as independent of, CLC-GFP, respectively. Taken together, these results strongly suggest the uptake of GPI-anchored proteins by both clathrin-dependent and -independent mechanisms in root epidermal cells.

A Ubiquitous Clathrin-Dependent Pathway and a Spatially Restricted Clathrin-Independent Pathway Operate in the Arabidopsis Root

We examined the effect of 1-naphthalene acetic acid (NAA), an inhibitor of clathrin-dependent endocytosis in plant cells (Paciorek et al., 2005; Robert et al., 2010), on endocytosis in the Arabidopsis root. In agreement with previous reports (Robert et al., 2010), NAA treatment reduces the localization of CLC-GFP to the PM as observed by both confocal and VAEM imaging (Supplemental Figures 4A to 4D). Moreover, we found that NAA treatment severely diminished the mobility and turnover of CLC-GFP foci. When we superposed two VAEM snapshots of CLC-GFP foci in control roots taken 20 s apart, several foci were seen in previously unpopulated areas while other foci were no longer seen in their original locations (Supplemental Figure 4B). However, in roots treated with NAA, such turnover was completely blocked. CLC-GFP foci in the VAEM images taken 20 s apart completely overlapped, and there was no evidence of either recruitment or loss of any clathrin foci (Supplemental Figure 4C). GFP-tagged versions of clathrin-dependent cargo, the auxin efflux carrier proteins PIN2 (epidermis and cortex; Xu and Scheres, 2005) and PIN1 (stele; Benková et al., 2003) as well as another transmembrane protein, LOW TEMPERATURE INDUCED-6B (LTI6b; all layers of root; Cutler et al., 2000), did not accumulate in BFA bodies following NAA treatment, demonstrating that the pathway was effectively blocked throughout the root (Supplemental Figure 4E). Thus, NAA pretreatment efficiently blocks the recruitment of clathrin to the PM and also the uptake of clathrin-dependent cargo from this membrane. However, the lipid probes GFP-GPI and SKU5-GFP, as well as FM4-64, accumulate in BFA bodies in epidermal cells even following NAA pretreatment (Figures 2A and 2C, right; Supplemental Figure 2C).

The average surface area of BFA bodies containing GFP-GPI or FM4-64 in the NAA-pretreated roots was about half that in roots treated only with BFA (Figures 2B and 2D), indicating that while a fraction of the lipid probes is taken up by a pathway that is refractory to NAA treatment, entry of a significant fraction of these lipid probes is in fact sensitive to NAA. This observation is corroborated by VAEM imaging, which showed a dramatic 50% reduction in the number of foci that contained both CLC-GFP and mCherry-GPI in the presence of NAA. By contrast, the occurrence of mCherry-GPI foci that are independent of clathrin was elevated by NAA treatment (Supplemental Figures 3B and 3D). In PIN2-GFP Arabidopsis roots treated with BFA, internalized FM4-64 accumulated in BFA bodies along with PIN2-GFP in cells of the epidermis and cortex (Figures 2E and 2F). However, when the roots were pretreated with NAA, FM4-64 but not PIN2-GFP accumulated in BFA bodies in the epidermal layer cells (Figures 2G and 2H), confirming the operation of an endocytic mechanism refractory to NAA in these cells. A similar observation was made in LTI6b-GFP plants; while NAA pretreatment blocked the uptake of LTI6b across all cell layers, the uptake of FM4-64 in BFA bodies could still be observed in epidermal cells (Supplemental Figure 5).

The uptake of lipid probes in BFA bodies following pretreatment with NAA was limited to epidermal cells and a few cells of the cortex at the root tip. BFA bodies containing GFP-GPI, FM4-64, or SKU5-GFP failed to accumulate in the morphologically distinct endodermis and stele of roots pretreated with NAA (Figures 2A and 2C, right, and Figure 2G, middle; Supplemental Figures 2C and 5B and Supplemental Movie 4), although they accumulated in all cell layers when the roots were treated with BFA alone (Figures 2A and 2C, left, and Figure 2E, middle; Supplemental Figures 2C and 5A and Supplemental Movie 5). It is conceivable that the entry of BFA into the stele cells may be reduced in the presence of NAA. Therefore, we observed the uptake and BFA-induced aggregation of FM4-64 in plants expressing the endosomal marker ARA7-GFP (Ueda et al., 2001). Internalized FM4-64 in stele cells accumulated in ARA7-GFP-labeled compartments (Supplemental Figure 6A), and upon BFA treatment, ARA7-GFP and FM4-64 clumped together in BFA bodies (Supplemental Figure 6B). With NAA pretreatment, we could still observe the formation of BFA bodies containing ARA7-GFP, establishing that BFA still reaches stele cells in the presence of NAA (Supplemental Figure 6C). These BFA bodies, however, were devoid of internalized FM4-64, demonstrating that internalization of FM4-64 was effectively blocked in these cells. Furthermore, we incubated wild-type plants with FM4-64 in the absence of BFA. After 30 min of pulse, we could observe the internalization of FM4-64 in punctate endosomal structures in stele (Supplemental Figure 6D, red arrows) as well as in the epidermis (green arrows). Pretreatment with NAA abrogated such FM-containing punctate structures in the stele, indicating a complete block in endocytosis (Supplemental Figure 6E, dashed area). Note, however, that the cell membranes remain outlined by FM4-64, demonstrating that the access of the dye to the stele is not compromised by NAA treatment. Uptake of FM4-64 could still be seen in the epidermal cells in the same image (Supplemental Figure 6E, green arrows), suggesting the functioning of a clathrin-independent pathway in those cells.

To directly address the role of clathrin in the uptake of the lipid probes, we expressed RFP-tagged HUB1 protein from a tamoxifen-inducible promoter to genetically perturb clathrin-dependent

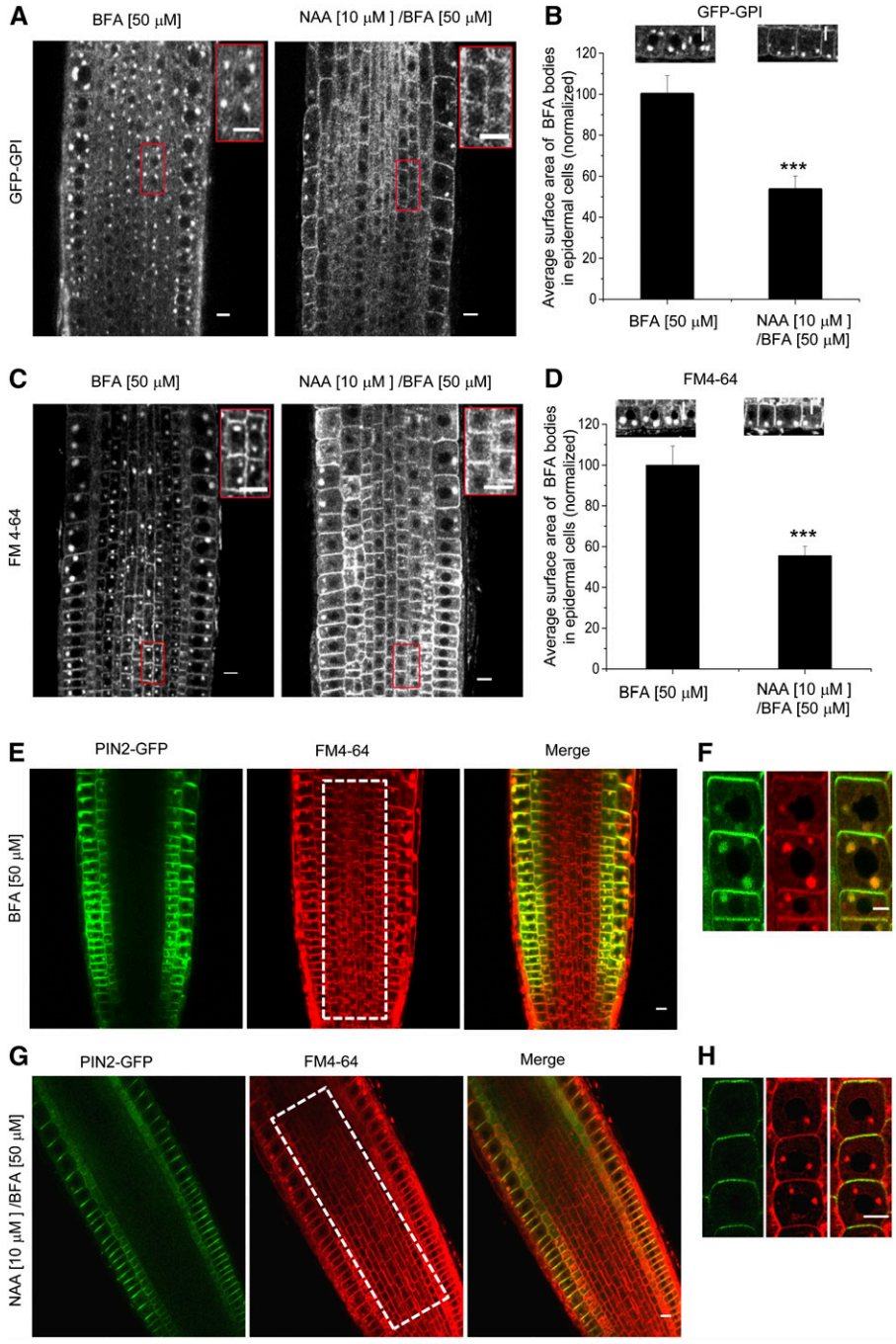

Figure 2. Effect of Clathrin Inhibition on Endocytosis.

(A) and **(C)** Uptake and BFA-induced aggregation of GFP-GPI **(A)** and FM4-64 **(C)** in Arabidopsis root in the absence (left) or in the presence (right) of NAA pretreatment. Insets represent magnified versions of the boxed areas.

(B) and **(D)** Quantification of the average surface area of BFA bodies containing GFP-GPI **(B)** and FM4-64 **(D)** in epidermal cells of plants in the absence or presence of NAA pretreatment. Bars represent weighted means of the surface area ± SE. Asterisks indicate $P < 0.0001$ (Student's *t* test). These results are based on three independent experiments with at least 150 BFA bodies quantified per group per experiment.

(E) to **(H)** Uptake and clumping of PIN2-GFP and FM4-64 in response to BFA treatment (**[E]** shows lower magnification and **[F]** shows higher magnification) or NAA + BFA treatment (following NAA pretreatment) (**[G]** shows lower magnification and **[H]** shows higher magnification). Stele cells in BFA-treated roots have clumps containing FM4-64, while those pretreated with NAA do not (**[E]** and **[G]**, boxed area in the middle panels).

Bars = 10 μm.

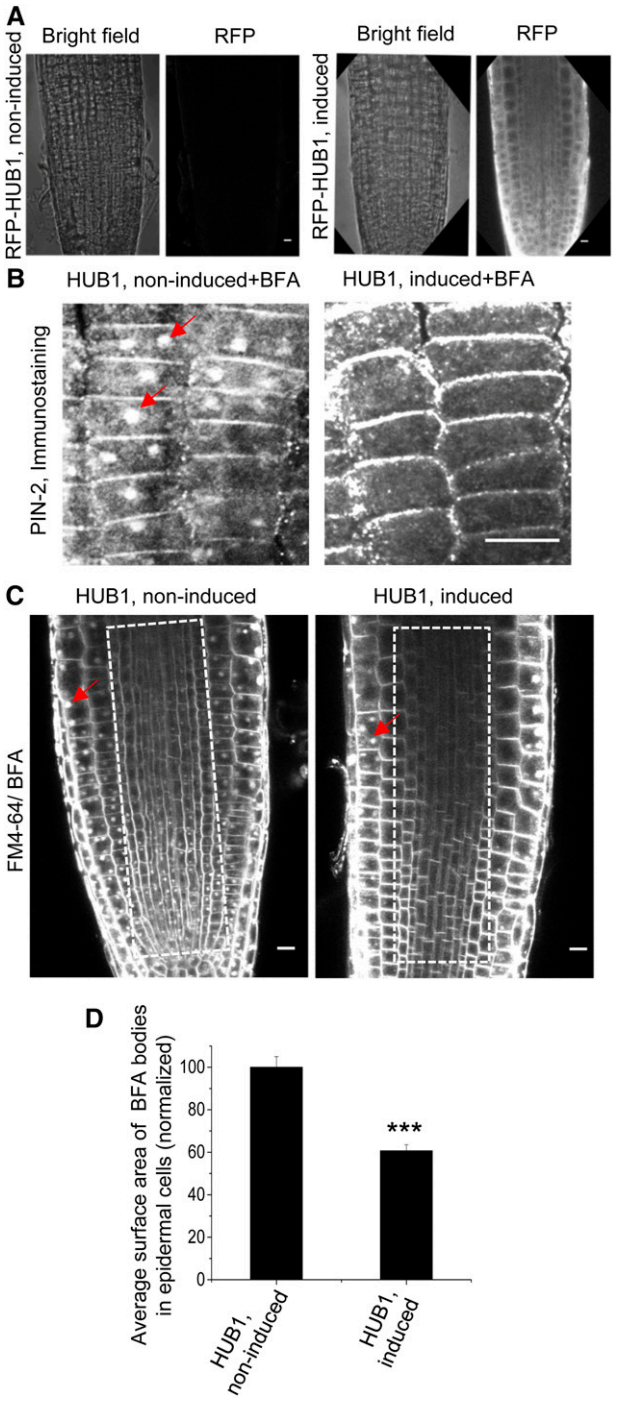

Figure 3. Inhibition of Clathrin-Dependent Endocytosis by HUB1 Expression.

(A) RFP-tagged HUB1 was expressed in pINTAM>>RFP-HUB1 plants induced with 2 μM 4-hydoxy tamoxifen for 30 h (right). No RFP expression could be seen in noninduced plants (left).

(B) Visualization of endogenous PIN2 by immunostaining in HUB1-RFP plants treated with BFA. PIN2 accumulates in BFA bodies in noninduced plants (left; arrows) but not in induced plants (right).

(C) In HUB1-expressing plants, FM4-64 uptake and BFA-induced clumping are seen in epidermal cells (right; arrow) but not in the inner cell layers (right; boxed area). FM4-64 uptake is seen in internal layers of noninduced plants (left; boxed area). Bars = 10 μm in **(A)** to **(C)**.

(D) Quantification of the average surface area of FM4-64-containing BFA bodies in epidermis of plants in the presence or absence of HUB1 induction. Bars represent weighted means ± SE. Asterisks indicate $P < 0.0001$ (Student's *t* test). These results are based on two independent experiments with at least 200 BFA bodies quantified per group per experiment.

endocytosis (Robert et al., 2010; Kitakura et al., 2011). Neither uptake nor BFA-induced clumping of PIN2 was observed in epidermal cells of plants following the induction of RFP-HUB1 (30 h) expression in all cell layers of the root (Figure 3A), consistent with the block of clathrin-dependent endocytosis in this layer (Figure 3B), in agreement with previous reports (Robert et al., 2010; Kitakura et al., 2011). While FM4-64-containing BFA bodies formed in all cell layers of the root of noninduced RFP-HUB1 plants (Figure 3C, left), no FM4-64-containing BFA bodies formed in the internal layers of the roots of tamoxifen-treated plants, indicating a complete block of all forms of endocytosis in these layers of cells (Figure 3C, right). The uptake of FM4-64 into BFA bodies was prominent in the epidermal layer of HUB1-induced plants (Figure 3C). Similar to the NAA treatment, the average surface area of these BFA bodies was markedly smaller compared with control cells (Figure 3D). Taken together, these data strongly suggest the functioning of a clathrin-independent endocytic pathway in the Arabidopsis root that is spatially restricted to the epidermal layer.

Further confirmation of these results was obtained using the small molecule tyrphostin-A23 (Tyr-A23), which inhibits receptor-mediated endocytosis in plants (Dhonukshe et al., 2007), presumably by preventing the recruitment of transmembrane cargo via the AP-2 adapter complex (Ortiz-Zapater et al., 2006) to clathrin-coated vesicles. Higher concentrations of Tyr-A23 might affect other adaptor complexes, leading to general defects of clathrin-dependent endocytosis (Konopka et al., 2008; Konopka and Bednarek, 2008; Fujimoto et al., 2010). We refrained from using higher concentrations of the inhibitor, as it affects the viability of plants over long incubation times. Pretreatment with Tyr-A23 (30 μM, 30 min) inhibited the uptake of PIN2-GFP but not that of GFP-GPI into BFA bodies in epidermal cells (Supplemental Figures 7A and 7D). We used dark-induced vacuolar accumulation of PM proteins as another assay for endocytosis (Kleine-Vehn et al., 2008; Laxmi et al., 2008). Incubation in darkness for 6 h resulted in the accumulation of both PIN2-GFP and GFP-GPI into vacuoles of epidermal cells (Supplemental Figures 7B and 7E, left). Tyr-A23 treatment (30 μM) inhibited the uptake and vacuolar accumulation of PIN2-GFP, while the vacuolar accumulation of GFP-GPI remained unaffected (Supplemental Figures 7B and 7E, right; quantification is shown in Supplemental Figures 7C and 7F). Surprisingly, Tyr-A23 did not block the uptake of GFP-GPI (Supplemental Figure 7D, right) or FM4-64 (Supplemental Figure 7G) in internal

cells like stele. BFA treatment caused the coaccumulation of LTI6b-GFP and FM4-64 in BFA bodies across all layers of the root (Supplemental Figures 7H and 7I). Tyr-A23 pretreatment blocked the uptake of LTI6b-GFP into BFA bodies across all the cell layers but did not block the cognate process for FM4-64 uptake in any of the cell layers (Supplemental Figures 7J and 7K). It would thus appear that the uptake of lipid probes like FM4-64 or GPI-anchored proteins does not require the Tyr-A23-sensitive components that are indispensable for the endocytosis of transmembrane proteins.

Clathrin-Independent Endocytosis Is Inhibited by Sterol Depletion

Clathrin-independent endocytosis of GPI-anchored proteins in animal cells is critically dependent on membrane sterol content (Chadda et al., 2007). Pretreatment with methyl-β-cyclodextrin (MβCD), a compound known to deplete sterol from the plant PM (Roche et al., 2008; Li et al., 2011), reduced FM4-64 uptake in epidermal cells (Figures 4A and 4B). However, the uptake of the clathrin-dependent transmembrane cargo LTI6b-GFP was unaffected (Figures 4C and 4D). Similarly, with VAEM imaging, we found that MβCD treatment markedly reduced the number of mCherry-GPI foci that were independent of CLC-GFP without significantly affecting the number of foci that colocalized with CLC-GFP (Supplemental Figures 3C and 3E). Hence, MβCD treatment specifically inhibits clathrin-independent endocytosis but does not affect the clathrin-dependent pathway. Furthermore, FM4-64 uptake, which was refractory to NAA treatment in the epidermal cells, was severely diminished in response to simultaneous sterol depletion by MβCD (Figure 4B). Thus, the clathrin-independent endocytosis operating in the epidermal cells is sensitive to sterol depletion.

Salinity Induces a Clathrin-Independent Bulk-Flow Endocytosis Pathway across All Layers of Arabidopsis Root

Exposure to salinity has been reported to enhance the endocytic uptake of FM dyes in root epidermal cells (Leshem et al., 2007; Li et al., 2011). Exposure to 100 mM NaCl significantly increased the number of clathrin-independent mCherry-GPI foci compared with the control (Supplemental Figures 3D and 3E). Similar treatment increased FM4-64 uptake by ~30% in root epidermal cells (Figures 5A and 5B), of which a significant part was due to NAA-insensitive uptake (enhancement of 50% even in the presence of NAA). It may be noted that NAA was just as effective in reducing the recruitment of CLC-GFP to the PM in the presence of saline stress as in its absence (Supplemental Figure 4A, right). Hence, the salt-induced enhancement of FM4-64 uptake in the presence of NAA may be ascribed to a clathrin-independent process. We also found that salinity increased FM4-64 uptake by 20% in epidermal cells of sterol-depleted (MβCD-treated) plants, indicating that uptake via the clathrin-dependent pathway is also enhanced, albeit by a smaller amount. Treatment with both NAA and MβCD together blocked all salt-induced increases in FM4-64 uptake. This observation indicates that all augmented and induced pathways are sensitive to one or the other of these reagents.

Two features distinguish the saline stress-induced endocytic pathway from the constitutive clathrin-independent pathway: cargo selectivity and the region of operation. Exposure of NAA-treated plants to 100 mM NaCl resulted in the uptake of GFP-GPI and FM4-64 into BFA bodies not only in the epidermis but also in the internal cell layers where NAA-insensitive clathrin-independent endocytosis is not normally observed (Figure 5C; Supplemental Figure 8A). Surprisingly, in response to salinity, despite NAA or Tyr-A23 pretreatment, the uptake of clathrin-dependent cargo like PIN2-GFP (in epidermal layers) and LTI6b-GFP (throughout the root) was also observed (Figures 5D and 5E; Supplemental Figure 8B). Plants expressing RFP-HUB1 and stressed with 100 mM NaCl also exhibited FM4-64 uptake in internal layers, unlike unstressed plants expressing RFP-HUB1, where the uptake of FM4-64 was blocked (Figure 5F).

Concurrent with the induction of this clathrin-independent endocytosis by salt stress in internal cell layers, we observed a notable increase in PM sterol content of these cells. We used the polyene dye filipin as a reporter of PM sterol levels (Grebe et al., 2003; Li et al., 2011). After 1 h of treatment with 100 mM NaCl, plants were cotreated with 100 μg/mL filipin for another 1 h. Under the same acquisition settings, the PMs of inner cell files of control plants showed very faint fluorescence, and cell outlines were barely visible (Figure 5G, middle, dashed box). The PMs of similar cells of salt-treated plants displayed much stronger fluorescence (Figure 5G, right, and Figure 5H). A similar observation was made in PIN1-GFP plants, where the PM of stele cells is marked with GFP (Supplemental Figure 9A). A 5 μM pulse of FM4-64 labeled PMs of inner cells of control plants and salt-treated plants equally (Supplemental Figures 9B and 9C), establishing that accessibility to the stele was not enhanced by salt stress. The importance of structural sterols in salt tolerance is further corroborated by the fact that the sterol methyltransferase-defective *smt2 smt3* double mutant plants (which have altered profiles of structural sterols but not brassinosteroids; Carland et al., 2010) showed marked salt sensitivity compared with wild-type plants (Supplemental Figures 10A and 10B). In addition, treatment with fenpropimorph, an inhibitor of the sterol C14 reductase FACKEL (He et al., 2003) and also an inhibitor of salt-induced endocytic response (Li et al., 2011), renders wild-type plants extremely salt-sensitive (Supplemental Figures 10E and 10F). We also found that the *smt2 smt3* plants were impaired in mounting the endocytic augmentation seen in wild-type plants (Supplemental Figures 10C and 10D).

The Salinity-Induced Clathrin-Independent Endocytic Response Is Impaired in the *vps9a-2* Mutant

The Rab-GEF VPS9a is a common activator of different Rab5 GTPases (Goh et al., 2007), which have been shown to be crucial regulators of both endocytosis and intracellular trafficking in plants (Kotzer et al., 2004; Ebine et al., 2011). The partial loss-of-function allele of *VPS9a*, known as *vps9a-2*, leads to diverse trafficking defects, such as defects in secretory as well as endocytic delivery of proteins to the vacuoles (Ebine et al., 2011; Inoue et al., 2013). The constitutive clathrin-independent pathway is functional in epidermal cells of *vps9a-2* plants, as shown by the formation of FM4-64-containing BFA bodies

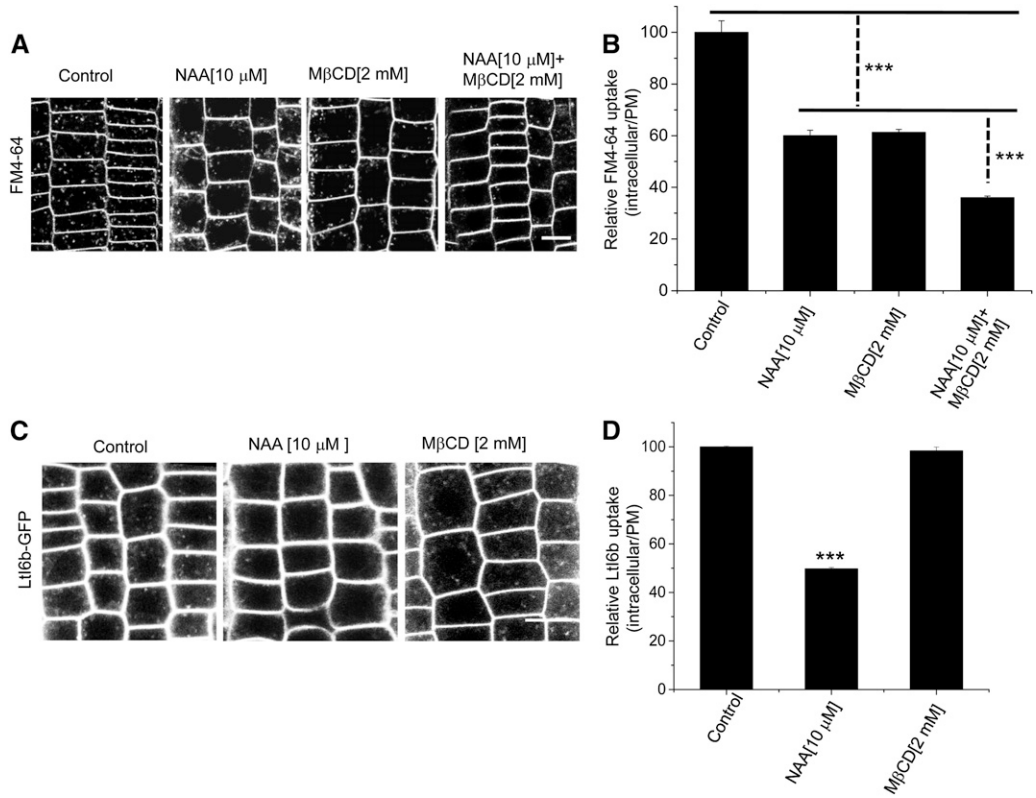

Figure 4. Both Clathrin-Dependent and Sterol-Sensitive Clathrin-Independent Endocytosis Operate in Epidermal Cells.

(A) Uptake of FM4-64 (30-min pulse with 5 μM dye) in epidermal cells of control plants or plants pretreated with 10 μM NAA, 2 mM MβCD, or 10 μM NAA + 2 mM MβCD. Bar = 10 μm.

(B) Quantification of FM4-64 uptake in control plants and inhibitor-treated plants. Bars indicate means ± SE. Asterisks indicate $P < 0.0001$ (Student's *t* test between groups). These results are averages of two independent experiments with at least 200 cells quantified per group per experiment.

(C) and **(D)** Uptake of transmembrane protein LTI6b-GFP in control plants and plants in the presence of 10 μM NAA and 2 mM MβCD. Bars represent means ± SE. Asterisks indicate $P < 0.0001$ (Student's *t* test). These results are based on two independent experiments with at least 200 cells analyzed per group per experiment. Bar = 10 μm.

following pretreatment with NAA (Figure 6A, middle). FM4-64 uptake in the epidermal cells of *vps9a-2* plants was enhanced by salinity, although to a smaller extent than in wild-type plants. However, pretreatment with NAA abrogated all salt-induced enhancement of FM4-64 uptake in epidermal cells of mutant plants (Figure 6B). Moreover, salinity-induced accumulation of FM4-64 in BFA bodies was not observed in internal cell layers of *vps9a-2* plants pretreated with NAA (Figure 6A, right), indicating that the salt-induced bulk-flow pathway is not operative in this mutant. Since the constitutive clathrin-independent pathway is unperturbed in *vps9a-2* plants, these findings suggest that VPS9a is a component of the salinity-induced clathrin-independent pathway but not the constitutive pathway.

We also observed a dramatic relocalization of VPS9a protein upon salt stress. VPS9a-GFP driven by its native promoter is present in the cytosol as well as intracellular endocytic compartments. However, in response to salt stress (100 mM NaCl, 45 min), we noted an almost 3-fold increase in the number of punctate intracellular compartments labeled with VPS9a-GFP in epidermal cells (Figures 6C and 6D). We found it difficult to quantify such bodies in internal cells, owing to their very small size. Moreover, we also found that at early time points after salt stress (30 to 45 min), the PM region of some cells displayed strong GFP fluorescence (Supplemental Figures 11B and 11D), a pattern not commonly observed in control plants (Supplemental Figures 11A and 11C). The enhanced membrane localization of VPS9a-GFP under salt stress was also supported by cell fractionation experiments, which revealed an enrichment of VPS9a-GFP in the membrane phase under salt stress compared with control conditions (Supplemental Figures 11E and 11F). Since such altered localization and activity of Rab5-GEFs are known to play a critical role in the activation of endocytic pathways in response to signaling cascades (Tall et al., 2001), it is not unreasonable to assume that VPS9a is involved in mediating the alteration of endocytosis in response to salt stress.

Expansion of Vacuolar Structures in Internal Layers Parallels Endocytic Reprogramming in the Internal Layers of the Root

In the meristematic region of control plants, only the epidermal layer has a well-developed and extensive vacuolar structure,

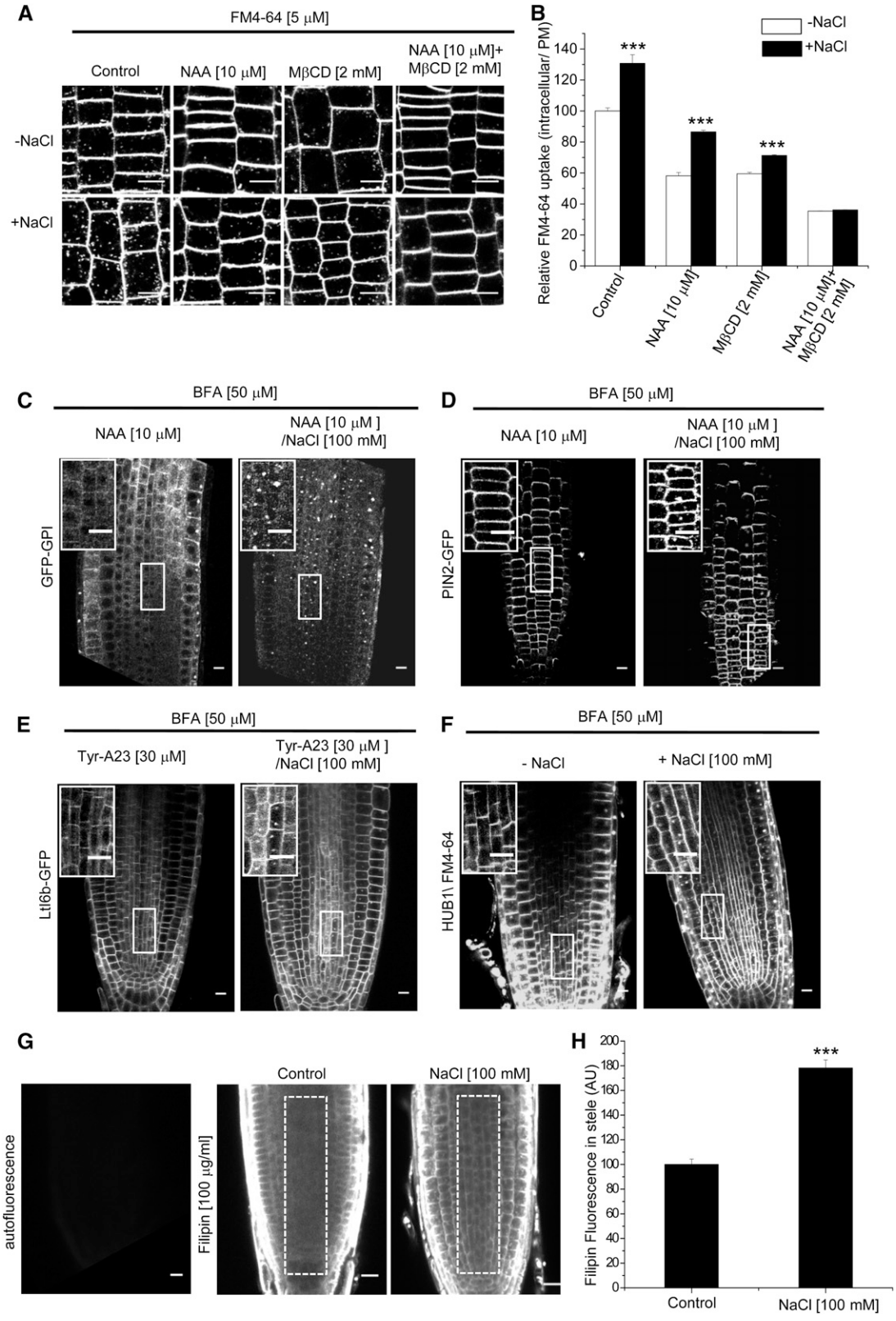

Figure 5. Salt Stress Induces a Clathrin-Independent Endocytosis Pathway in Arabidopsis Root.

with rather smaller vacuoles seen in the cortex (Hamaji et al., 2009). Staining roots with LysoTracker Red, which stains acidic compartments (Laxmi et al., 2008), recapitulated these earlier findings (Figure 7A). No large vacuole-like bodies accumulated stain in endodermis or stele, which have small, dispersed acidic vesicles (Figure 7A, right). However, on treating the plants with 100 mM NaCl for 24 h, vacuolar structures in the cortex became more extensive, consistent with previous reports (Hamaji et al., 2009). In addition, large acidic compartments, reminiscent of vacuoles, were seen in the endodermis and the stele (Figure 7B, right). In the stele region, the vacuolar area increased almost 2.5-fold (from 22% of stele cells under control conditions compared with 56% of the cellular area after 24 h of salt stress) in response to salt (Figure 7E). We also observed the vacuolar structures in the stele using the GFP-tagged form of the vacuolar SNARE SYP22 (Hamaji et al., 2009); salt stress for 24 h caused a similar expansion of vacuolar structures marked with SYP22-GFP in stele cells (Supplemental Figure 12) compared with control plants, where the vacuoles in stele cells appear to be organized in thin tubular structures (Viotti et al., 2013). Intriguingly, in the *vps9a-2* mutant, wherein induction of salt-induced clathrin-independent endocytosis is inhibited, salinity-induced development of vacuolar structures in the inner cell layers was also not observed (Figures 7C to 7E). Thus, vacuolar structures that are uniformly induced across all cell layers under salinity stress clearly correlate with the induction of a VPS9a-regulated clathrin-independent endocytic mechanism in these layers.

Finally, these processes are likely to be functionally important for combating saline stress, since *vps9a-2* plants are acutely salt-sensitive compared with wild-type plants. Root growth under 100 mM NaCl stress is severely curtailed in *vps9a-2* plants compared with wild-type plants (Figure 7H). Ten days of stress with 100 mM NaCl is lethal for *vps9a-2* plants, while the wild-type plants stay viable under similar conditions (Figure 7F). Intriguingly, severe drought stress (half-strength Murashige and Skoog [MS] agar perfused with 400 mg/mL polyethylene glycol [PEG] 6000) (Verslues et al., 2006) that hindered the growth of wild-type plants to an almost similar extent to saline stress did not kill the *vps9a-2* plants. Although the growth of the *vps9a-2* plants was severely affected by drought, the plants generated true leaves, unlike salt-treated plants, which became bleached and did not generate true leaves. Root growth of *vps9a-2* plants was much more affected by salt than by drought stress (Figure 7G versus Figure 7H). Thus, it would appear that the salt sensitivity of *vps9a-2* is a specific phenotype and does not result from pleiotropic growth defects.

DISCUSSION

Vesicle trafficking involves a large number of precisely orchestrated components that have been best characterized in studies of clathrin-mediated endocytosis in animal cells (Taylor et al., 2011). However, studies describing variations in endocytic mechanisms across different cell types of mature functioning organs are scarce, mainly because of the inaccessibility of deeper tissue layers to optical microscopy. The Arabidopsis root is a well-stratified organ composed of distinct cell layers that are clearly demarcated in terms of position, shape, and developmental origin (Scheres et al., 2002). Gene expression profiles in these different cell types differ and are differentially perturbed under environmental stress (Birnbaum et al., 2003; Dinneny et al., 2008). All layers of the small, transparent root are amenable to light microscopy; thus, it provides an ideal system for the study of endocytic mechanisms across different cell layers of an intact, functioning tissue.

The only well-characterized endocytic pathway in plants is the clathrin-dependent pathway, mostly due to the availability of specific chemical inhibitors, NAA and Tyr-A23, and the genetically inducible HUB1, which acts as a dominant negative inhibitor of clathrin function (Dhonukshe et al., 2007; Kitakura et al., 2011). Each of these perturbations effectively blocks the uptake of all transmembrane proteins so far examined by us (PIN2-GFP, LTI6b-GFP, and PIN1-GFP), confirming that these proteins are taken up exclusively by a clathrin-dependent pathway. We find that this pathway operates constitutively in all layers of the root.

GPI-anchored proteins are endocytosed in animal cells by a pathway that is independent of coat proteins, including clathrin (Sabharanjak et al., 2002). We have generated a reporter for this pathway by linking fluorescent protein tags to a conserved plant-specific GPI anchorage sequence (Eisenhaber et al., 2003). The intracellular distribution, as well as the trafficking properties of the resulting reporters, are identical to those of the

Figure 5. (continued).

(A) and **(B)** FM4-64 uptake in epidermal cells of control and inhibitor-treated plants in the presence and absence of salt stress. FM4-64 uptake was quantified after a 30-min pulse with 5 μM dye in control plants and plants pretreated with NAA, MβCD, and NAA + MβCD followed by cotreatment with NaCl (30 min) in the case of salt-stressed plants. Error bars represent SE. Asterisks represent $P < 0.0001$ (Student's *t* test between groups). These results are cumulative of two independent experiments with at least 200 cells analyzed per group per experiment.

(C) and **(D)** Uptake and BFA-induced aggregation of GFP-GPI **(C)** and PIN2-GFP **(D)** in the presence of NAA (left) or NAA + NaCl (right).

(E) Uptake and BFA-induced clumping of LTI6b-GFP in the presence of Tyr-A23 (left) or Tyr-A23 + NaCl (right).

(F) FM4-64 uptake in HUB1-RFP (30-h induction)-expressing roots in the absence (left) and presence of NaCl (right).

(G) Filipin staining of Arabidopsis root. Left, autofluorescence; middle and right, control and salt-treated plants stained with filipin. The stele is marked by the dashed boxes.

(H) Quantification of filipin fluorescence in the stele region of control and salt-treated plants. These results are cumulative of two independent experiments with a total of 20 plants quantified per group. Asterisks represent $P < 0.0001$ (Student's *t* test).

Insets are magnified versions of the boxed areas in **(C)** through **(F)**. Bars = 10 μm.

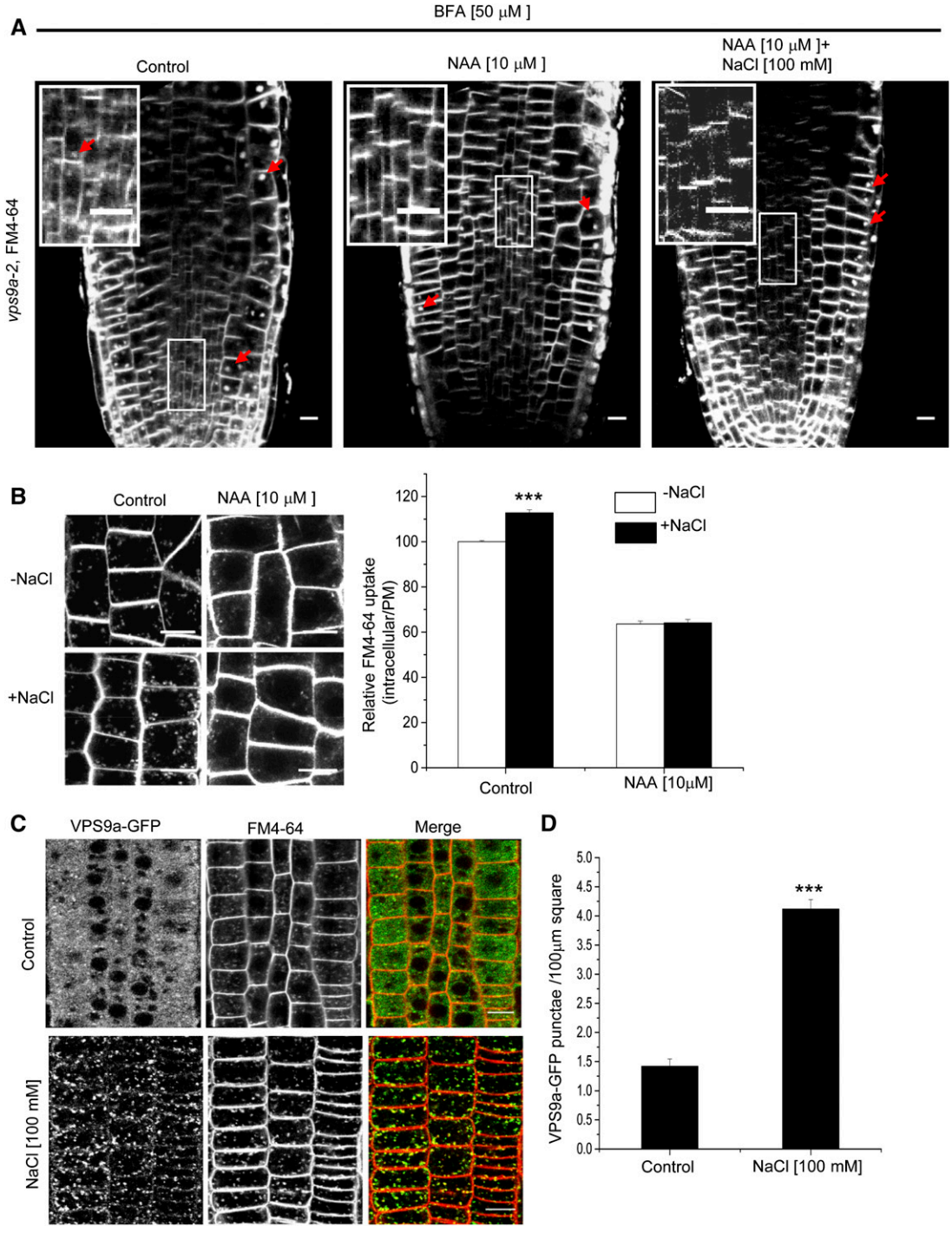

Figure 6. VPS9a Is Involved in Salt-Induced Bulk-Flow Endocytosis.

(A) Accumulation of FM4-64 in BFA bodies across layers of *vps9a-2* root in control plants (left), with NAA pretreatment (middle), and with NAA + NaCl pretreatment (right). Insets are magnified versions of the boxed areas.

(B) FM4-64 uptake (5 μM, 30-min pulse) in epidermal cells of control and NAA-treated *vps9a-2* roots in the presence and absence of 100 mM NaCl. Error bars represent SE. Asterisks represent $P < 0.0001$ (Student's *t* test). These results are sums of data from two independent experiments with at least 200 cells analyzed per group per experiment.

(C) Salt-induced change in VPS9a-GFP localization. Control plants (top) or plants treated with 100 mM NaCl (bottom) were subsequently cotreated with 5 μM FM4-64 for 30 min. Salt treatment causes a substantial increase in the number of intracellular punctae labeled with VPS9a-GFP.

endogenous and functional GPI-anchored protein SKU5 (Supplemental Figure 2) (Sedbrook et al., 2002). The endocytosis of GFP-GPI parallels that of FM4-64-impregnated membrane in all contexts that we have examined so far. Thus, our probe serves as a genetically encoded reporter for GPI-anchored proteins in particular and lipids in general.

Endocytosis of GPI-anchored proteins and FM4-64 was observed in all cell layers of the Arabidopsis root. Blocking clathrin-mediated endocytosis by either NAA or HUB1 expression reduced the size of BFA bodies labeled with these lipid probes without eliminating their formation in cells of the epidermis and a few cells of the cortex very close to the root tip. These latter cells are morphologically part of the cortex but are close to the stem cell niche and do not express some cortical markers expressed in older cells (Birnbaum et al., 2003). It is conceivable that they are still in the process of adopting a cortical identity. Nevertheless, these observations indicate that FM4-64 and GFP-GPI are constitutively endocytosed by both clathrin-dependent and -independent pathways in the epidermis and very young cortical cells. By contrast, in the inner cell layers, such as the endodermis and stele, clathrin perturbation by multiple means (HUB1 expression and NAA) abrogates the accumulation of BFA bodies for both the lipid probes (GPI-anchored proteins and FM4-64), suggesting that the endocytic uptake in the inner cell layers consists of only a clathrin-dependent endocytic pathway.

BFA can indirectly affect the rate of endocytosis by causing an agglomeration of TGN and by blocking recycling as well as vacuolar trafficking depending upon the dosage (Kleine-Vehn et al., 2008). Indeed, BFA induced an upregulation of fluid phase endocytosis in animal cells (Kumari and Mayor, 2008), and an upregulation of FM4-64 uptake in *Picea meyeri* pollen tubes is documented (Wang et al., 2005). VAEM imaging, a technique that has been employed extensively to study the dynamics and internalization of membrane coat proteins as well as transmembrane cargo (Konopka et al., 2008; Konopka and Bednarek, 2008; Fujimoto et al., 2010; Li et al., 2011) in the epidermal cell layer, provides a parallel and complementary validation of these conclusions. VAEM imaging of root epidermal cells showed that mCherry-GPI was concentrated in two kinds of foci that build up at the cell surface. Around 60% of these colocalized with CLC-GFP and appear to be sensitive to NAA treatment; NAA caused a marked reduction in the number of mCherry-GPI foci that colocalize with clathrin. The remaining foci, which contain only mCherry-GPI, were sensitive to the removal of sterol, consistent with the functioning of a sterol-dependent but clathrin-independent endocytosis pathway in the epidermal cells.

Several reports of clathrin-independent endocytic pathways taking up fluorescent nanobeads, glucose analogs, or gold nanoparticles in plant cells have appeared (Onelli et al., 2008; Bandmann et al., 2012). However, no detailed mechanistic insight into such pathways has been presented. Moreover, these studies have been performed on cultured cells grown in the presence of high concentrations of auxins, which deviates from the normal physiological context. A detailed study of a clathrin-independent flotillin-mediated endocytic pathway in Arabidopsis was published recently (Li et al., 2012). However, neither the range of operation of the process nor the candidate cargo for the pathway was explored in that study. While the uptake of most GPI-anchored proteins is independent of flotillin in animal cells (Langhorst et al., 2008), the cognate mechanism has yet to be tested in plants and could be of interest for future studies. Our data establish that all constitutive clathrin-independent pathways are restricted to the epidermis and a few cells of the cortex. This pathway handles membrane lipid and lipid-anchored cargo, such as GPI-anchored proteins, but not transmembrane proteins.

We find that the constitutive clathrin-independent pathway is sensitive to sterol depletion by MβCD, as in animal cells (Chadda et al., 2007), whereas the uptake of transmembrane proteins and the recruitment of GPI-anchored proteins to clathrin-coated pits are unaffected (Figures 4A and 4B; Supplemental Figure 4C). The specific factors responsible for restricting the operation of the clathrin-independent pathway to the outer layers of the root are not currently known. However, sterol-modifying enzymes that regulate endocytosis, like SMT3, SMT2 (Carland et al., 2002), and CYCLOPROPYL ISOMERASE1 (Men et al., 2008), are preferentially expressed in outer cell layers compared with the inner cell layers (Dinneny et al., 2008), leading to the speculation that differences in PM lipid composition between cell layers may underlie this range restriction. Enhanced filipin staining of PM sterols in the epidermal layers compared with the inner cell layers provides some evidence for this speculation. We observe that the enhanced rate of endocytosis triggered by saline stress is not observed in *smt2 smt3* mutant plants. Furthermore, it is reported that fenpropimorph-treated wild-type plants show similar endocytic defects in response to salinity (Li et al., 2011). These observations together highlight the crucial role of membrane structural sterols in mounting the endocytic response to salt stress. Interestingly, the defective endocytic responses in the *smt2 smt3* mutant and fenpropimorph-treated wild-type plants are also accompanied by acute salt sensitivity. However, due to the diverse and crucial functions of structural sterols in cellular processes, other vital functions might also be impaired, culminating in salt sensitivity.

Endocytic pathways are subject to regulation by various external stimuli. Endocytic uptake helps plants to fine-tune the distribution of transporters and signaling molecules on the PM, which in turn helps plants to cope with situations like high boron or ammonium toxicity (Takano et al., 2005; Wang et al., 2013) or

Figure 6. (continued).

(D) Quantification of VPS9a-GFP intracellular punctae. The numbers of punctae at the midplane of the cells were counted by automatic particle detection (see Methods). These results are cumulative of three independent experiments with a total of 798 cells counted for control and 762 cells counted for salt treatment. Error bars represent SE. Asterisks represent $P < 0.0001$ (Student's *t* test).
Bars = 10 μm.

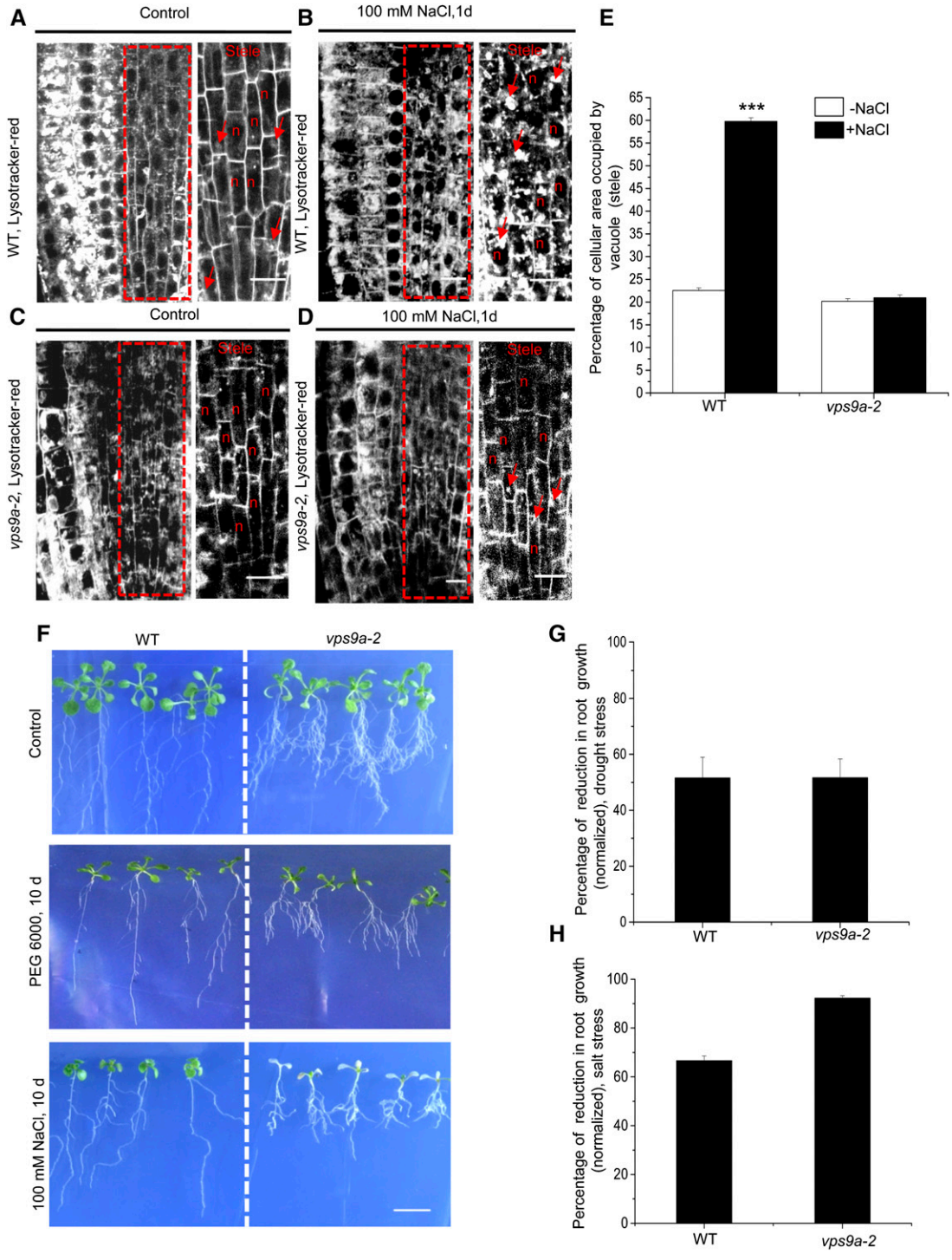

Figure 7. Salt-Induced Vacuole Development Is Impaired in the *vps9a-2* Mutant.

(A) and **(B)** Visualization of vacuolar structures across different layers of wild-type Arabidopsis root by staining with LysoTracker Red in unstressed plants **(A)** and plants stressed with 100 mM NaCl for 1 d **(B)**.

(C) and **(D)** Visualization of vacuolar structures in *vps9a-2* roots in unstressed plants **(C)** or plants treated with 100 mM NaCl for 1 d **(D)**.

Dashed boxes in **(A)** through **(D)** mark the stele. Right columns are magnified images from the stele region. Arrows indicate vacuolar structures. n, nucleus. Bars = 10 μm.

gravitropic stimulation (Kleine-Vehn et al., 2008). Salinity is a common abiotic stress to which plants mount a range of responses at the cellular and whole-plant levels. Salt stress is known to cause a dramatic increase in endocytic uptake (Leshem et al., 2007; Luu et al., 2012), resulting in the generation of intravesicular reactive oxygen species that act as second messengers in salt stress-elicited signaling pathways (Leshem et al., 2007; Golani et al., 2013). Salt stress is reported to elicit enhanced uptake and recycling of PM aquaporins in Arabidopsis root epidermis (Li et al., 2011; Luu et al., 2012). Such enhanced uptake is postulated to be partially due to the induction of a sterol-sensitive (lipid raft-dependent) pathway, which is not responsible for the uptake of aquaporins under control conditions. In addition, the salt-induced upregulation of PIN2-GFP uptake in epidermal cells in the presence of inhibitors that abolish clathrin recruitment to the PM has been described (Galvan-Ampudia et al., 2013). Our data support these previous and contemporary findings. Of the constitutive pathways, the clathrin-dependent pathway is mildly augmented under salt stress (Figure 5B), whereas the constitutive clathrin-independent pathway in epidermal cells does not appear to be affected by NaCl stress. In addition, a sterol-sensitive clathrin-independent pathway is induced across all layers of the root. Unlike the constitutive clathrin-independent pathway(s) extant in epidermal cells, the salt-induced mechanism is not restricted to lipids but also takes up a variety of transmembrane proteins. We found a marked increase in the sterol content of the PMs of internal cells in response to salt stress. Cells in the stele normally have very little filipin-staining material in their PM, as opposed to epidermal cells, which stain brightly. Augmenting the sterol content in the endodermis and stele could be a crucial requirement for the induction of the sterol-sensitive bulk-flow endocytosis in these cell layers. Salt thus induces a reprogramming of endocytic pathways in the Arabidopsis root, blurring the sharp distinction between the epidermis and internal layers, with all cell layers exhibiting a uniform clathrin-independent pathway that takes up transmembrane as well as lipid-anchored cargo.

The salt-induced bulk-flow pathway further differs from the constitutively operating clathrin-independent pathway in that only the former is critically dependent on the Rab-GEF VPS9a, which is an activator of plant Rab-GTPases involved in endocytosis, especially the conventional Rab5 analogs ARA7 and RHA1 (Goh et al., 2007; Ebine et al., 2011). Whereas the complete loss of function of this gene is lethal, the partial loss-of-function allele *vps9a-2* displays defects in endocytosis (Inoue et al., 2013). While transcript levels of *VPS9A* are only moderately upregulated by saline stress, transcript levels of the Rab-GTPase genes regulated by VPS9a (*ARA6*, *ARA7*, and *RHA1*) are greatly enhanced by salinity, especially in the inner layers of the root such as the stele (Dinneny et al., 2008), suggesting a possible role of these players in the endocytic response to saline stress. The absence of the salt-induced bulk-flow pathway in *vps9a-2* plants supports this idea. We observed an enhanced vesicular as well as PM localization of VPS9a-GFP at early time points after salt stress. Recent studies have shown that the membrane localization and activity of Rab-GEFs are crucial factors in regulating the localization and specificity of downstream Rab-GTPases (Blümer et al., 2013; Cabrera and Ungermann, 2013). Rab-GEFs are also subject to activation by signaling cascades that regulate their membrane localization and subsequent endocytosis events (Tall et al., 2001). The enhanced PM and vesicular localizations of VPS9a suggest a potential molecular mechanism for the induction of salt-induced endocytosis and vacuolar expansion. Among the downstream targets of VPS9a, the plant-specific Rab5, ARA6, is palmitoylated (Ebine et al., 2011), which is likely to increase its association with regions of the membrane that have liquid-order-like properties (Smotrys and Linder, 2004). In fact, ARA6 is localized to PM domains that are well separated from clathrin foci and presumably could be associated with such domains. More importantly, salt stress strongly promotes the PM localization of a GTP-locked version of ARA6 (Ebine et al., 2011), and it could be a crucial target of the VPS9a-mediated salt-induced bulk-flow endocytosis. However, these observations need to be followed up with further experiments, and clearly, there must be other targets of VPS9a, since the salt sensitivity of the *ara6* mutant is much milder than that of *vps9a-2*.

In the meristematic region of the root, epidermal cells have a large vacuole that occupies much of the cell, while the cortex displays smaller vacuoles, and inner cell layers exhibit only small, fragmented acidic compartments. This distinct morphological differentiation mirrors the epidermal/internal layer schism. We speculate that there could be a correlation between the generation of mature vacuoles and the operation of the clathrin-independent endocytic pathways. Under control conditions (normal salt), both the constitutive operation of clathrin-independent endocytosis and the presence of well-developed vacuoles are restricted to the epidermal layer. By contrast, under saline stress, the induction of the VPS9a-sensitive clathrin-independent endocytic process throughout the root correlates

Figure 7. (continued).

(E) Quantification of the cellular area occupied by the vacuole in wild-type and *vps9a-2* plants under control conditions or after 1 d of stress with 100 mM NaCl. Bars represent weighted means of the percentage of cellular area occupied by vacuoles ± SE. Asterisks indicate $P < 0.0001$ (Student's *t* test). Plotted data are sums of two independent experiments with at least 100 cells quantified per genotype per condition.

(F) Four-day-old wild-type and *vps9a-2* plants were transferred to plates containing half-strength MS medium (top), half-strength MS medium perfused with 400 mg/mL PEG 6000 (middle), or half-strength MS medium supplemented with 100 mM NaCl (bottom). After 10 d, salt-treated *vps9a-2* plants start to die, while the wild-type plants remain relatively unaffected. Bar = 1 cm.

(G) and **(H)** Percentage reduction of root growth in response to drought stress (400 mg/mL PEG 6000, 10 d) **(G)** and salt stress (100 mM, 10 d) **(H)** in wild-type and *vps9a-2* plants compared with plants grown under control conditions. The root growth of 24 plants was quantified for each genotype/condition combination.

with the development of large vacuolar structures in the inner layers. Vacuolar Na^+/H^+ antiporters have been shown to play a significant role in ameliorating saline stress by accumulating Na^+ into the vacuole (Apse et al., 1999), thereby maintaining low cytosolic Na^+ (Anil et al., 2007). A large vacuolar volume is a prerequisite for such a role. Indeed, the loss of VPS9a function, which results in the inability to form a vacuolar system in the inner layers, also makes the plants extremely sensitive to saline stress. Apart from roles in endocytic uptake, VPS9a plays a crucial role in intracellular trafficking as well, such as protein transport to the vacuole (Ebine et al., 2011). In plants, the effectors of endocytosis, including the Rab5 GTPases (also known as RabF2 GTPases in Arabidopsis), have closely intertwined roles in intracellular trafficking as well as in endocytic uptake. For example, a mutant version of ARA7 has been shown to lead to defects in endocytosis (Robert et al., 2010) as well as in biosynthetic trafficking to the vacuole (Kotzer et al., 2004). It is plausible, therefore, that the endocytic defect manifested by the *vps9a-2* mutant is an indirect consequence of the defects in intracellular trafficking. Thus, both of these processes could be equally important in mediating the salt-response mechanisms regulated by VPS9a. Vacuolar trafficking plays a crucial role in salinity tolerance, as evidenced by multiple studies in which the alteration of expression levels of vacuolar trafficking regulators confers salt tolerance or sensitivity to plants (Mazel et al., 2004; Leshem et al., 2006; Kim and Bassham, 2011). Causal links between salinity-induced endocytic processes, vacuolar trafficking, and the formation of vacuolar compartments call for further investigation, as does the intriguing possibility that these processes may have survival value for plants under saline stress. Regardless, these studies establish functional roles for clathrin-independent endocytic pathways in metazoans (Mayor et al., 2014).

METHODS

Construction of the GFP/mCherry-GPI Expression Cassette

A 75-nucleotide GPI anchor signal sequence from the *Arabidopsis thaliana* gene COBRA (At5g60920) was PCR-amplified from Arabidopsis genomic DNA using the following primers: forward primer 5′-AACGGTGGTTCCCG-3′ and reverse primer 5′-TTAGGCAGAGAAGAAG-3′. The resulting PCR product was cloned in the pBI121 binary plasmid (for GFP-GPI) or ImpGWB502Ω (for mCherry-GPI). In the resulting cassette, GFP/mCherry contains an N-terminal signal peptide derived from an Arabidopsis vacuolar basic chitinase and a C-terminal 25-amino acid GPI-anchoring signal sequence (Eisenhaber et al., 2003). The cassette was expressed under the control of the cauliflower mosaic virus 35S promoter and NOS terminator. Transgenic Arabidopsis plants and tobacco (*Nicotiana tabacum*) BY-2 cells expressing the cassette were produced by *Agrobacterium tumefaciens*-mediated transfection.

Plant Materials and Growth Conditions

Arabidopsis seedlings and tobacco BY-2 cells were maintained as described before (Dhonukshe et al., 2007; Onelli et al., 2008). The *smt2 smt3* (Carland et al., 2010) and *vps9a-2* (Goh et al., 2007) mutant plants and Arabidopsis lines transformed with PIN2:PIN2-GFP (Xu and Scheres, 2005), 35S:LTI6b-GFP (Cutler et al., 2000), pINTAM>>RFP-HUB1 (Robert et al., 2010), CLC2:CLC-GFP (Konopka et al., 2008), ARA6:ARA6-GFP and ARA7:ARA7-GFP (Goh et al., 2007), SYP22:SYP22-GFP (Hamaji et al., 2009), UBQ10:SYP32-RFP (Geldner et al., 2009), and SKU5:SKU5-GFP/*sku5* (Sedbrook et al., 2002) have been described before. Vps9a: VPS9a-GFP/*vps9a-1* and pin1:PIN1-GFP lines were gifts from Takashi Ueda and Kalika Prasad, respectively.

Inhibitor Treatments of Plants

Four-day-old BY-2 cell suspensions or 4-d-old Arabidopsis seedlings were incubated in liquid MS medium (half-strength MS for plants) containing inhibitors or equal amounts of solvents (controls) as described in previous reports. Inhibitors were diluted from a 1000× stock and were used in the following final concentrations: BFA (Sigma-Aldrich; 50 μM; Paciorek et al., 2005), NAA (Sigma-Aldrich; 10 μM; Robert et al., 2010), Tyr-A23 (Sigma-Aldrich; 30 μM; Dhonukshe et al., 2007), 4-hydroxy tamoxifen (Sigma-Aldrich; 2 μM; Kitakura et al., 2011), and MβCD (Sigma-Aldrich; 2 mM; Li et al., 2011). The concentrations and incubation times for inhibitors of clathrin-mediated endocytosis (NAA and Tyr-A23) were determined by the necessity to maintain the viability of plants while blocking the uptake of clathrin-dependent cargo completely. For example, Tyr-A23 was used at 30 μM concentration to keep the plants viable over the 6-h incubation time for the vacuolar accumulation experiment. The MβCD concentration was titrated such that PM labeling by FM4-64 was not affected. Where inhibitors were used along with BFA, a pretreatment of the inhibitor alone was given for 30 min at the indicated concentrations followed by a 60-min cotreatment with inhibitor and BFA. In salinity-related experiments, plants were pretreated with the indicated inhibitors for 15 min following supplementation with 100 mM NaCl for 30 min and then further incubated for 60 min after the addition of 50 μM BFA. For fenpropimorph treatment, seeds were germinated on half-strength MS plates containing 20 or 50 μg/mL fenpromimorph (Sigma-Aldrich). Three days after germination, plants were transferred to half-strength MS plates containing the same concentration of fenpropimorph supplemented with or without 100 mM NaCl and grown for the indicated period.

PIN2 Immunostaining

Immunostaining of PIN2 was done as described before (Sauer et al., 2006) with a 1:1000 dilution of chicken anti-PIN2 (Agrisera) and a 1:500 dilution of Alexa-568-labeled goat anti-chicken (Jackson Immunoresearch) antibodies.

Total Membrane Isolation and VPS9a-GFP Immunoblotting

To probe the enhanced membrane association of VPS9a-GFP under salt stress, ~200 4-d-old VPS9a-GFP seedlings were treated with half-strength MS medium containing 100 mM NaCl for 30 min (salt-stressed) or only half-strength MS medium (control). Plants were then ground in homogenization buffer (25 mM HEPES-KOH, pH 7.5, 100 mM KCl [or 100 mM NaCl for salt-stressed plants], 10 mM $CaCl_2$, 10 mM $MgCl_2$, protease inhibitor cocktail [Sigma-Aldrich], and phosphatase inhibitor cocktail [Sigma-Aldrich]) using quartz powder (Sigma-Aldrich). The homogenate was centrifuged at 10,000*g* for 15 min, following which the supernatant was further centrifuged at 100,000*g* for 1 h to obtain the total membrane pool as pellet. After resuspension, the same amounts of protein from the control and salt-stressed pellets were loaded onto an SDS-PAGE apparatus and probed with anti-GFP (as a proxy for VPS9a-GFP) and anti-PM ATPase (Agrisera; as a loading control) antibodies.

Confocal Microscopy

Arabidopsis roots and BY-2 cells were imaged with an Olympus FV1000 confocal microscope (60× oil-immersion objective; numerical aperture, 1.35). Both GFP and FM4-64 were excited using a 488-nm laser. The

fluorescence emission spectra were separated with a 560LP dichroic mirror. GFP fluorescence was collected in the range of 495 to 540 nm, and that of FM4-64 was collected in the range of 570 to 650 nm. Alexa-568, RFP, mCherry, and LysoTracker Red were imaged by a 543-nm laser, and the emission fluorescence of Alexa-568, RFP, and LysoTracker Red was collected in the range of 580 to 620 nm and that of mCherry in the range of 600 to 650 nm. Filipin was excited by a 405-nm laser, and fluorescence emission was collected in the range of 420 to 490 nm. The colocalization analysis and determination of Pearson's coefficient were done using the ImageJ intensity correlation analysis plugin (Li et al., 2004).

VAEM Imaging and Quantification of Foci

Arabidopsis plants dually transformed with CLC2:CLC-GFP and 35S:mCherry-GPI were imaged with an inverted fluorescence microscope (Nikon Eclipse TE2000-E and a CFI Apo TIRF 100 × H/1.49 numerical aperture objective) with the TIRF2 system (Nikon). GFP and mCherry were excited with 488- and 561-nm lasers, respectively. The fluorescence emission was separated with a 565LP dichroic mirror and collected through either a 515/530BP (for GFP) or 580LP (for mCherry) filter in a dual-view filter system (Photometrics) and an iXonEM EMCCD camera (Andor). Each frame was exposed for 300 ms. For the quantification of GFP and mCherry foci (Supplemental Figures 3 and 4), first frames of 10 separate movies from three independent repeats were exported as TIFF files. Movies were selected not to contain intracellular punctate structures that showed unidirectional streaming movement as well as to contain foci whose area was above 100 μm^2 to rule out larger TGNs (Konopka et al., 2008). The green and red channel images were opened in Fiji software (http://fiji.sc/Fiji) and background subtracted with a 20-pixel-diameter rolling-ball filter. Individual foci were identified using the MOSAIC plugin of Fiji/ImageJ (Sbalzarini and Koumoutsakos, 2005). Circular foci that were three pixels in radius and with mean intensity in the upper 10th percentile of the image intensity distribution were chosen for analysis. The coordinates of the detected foci were recorded in the region of interest (ROI) manager using a custom-written Fiji macro.

For counting the number of foci that contained both GFP and mCherry, ROI information of all the foci in green and red channels was combined separately using the OR function, and then these combined green and red ROIs were overlaid using the AND function. The resulting ROIs represent the common area covered by both green and red foci. These new ROIs were loaded onto a new image of the same dimension. After space filling and converting the image into a binary mask, the number of foci was counted by the automatic particle detection tool provided within the Fiji software package (the minimum size threshold for detecting a particle was kept at three pixels, radius of a focus). Only green and only red foci were counted by subtracting the number of these combined foci from the total number of green and red foci for each frame. The average number of foci per 100 μm^2 was used to plot the graphs in Supplemental Figures 3E and 4D.

FM4-64 Uptake Quantification and Statistical Analysis

For the quantification of FM4-64 uptake, plants were pulsed with 5 μM FM4-64-X (Invitrogen) for 30 min in liquid half-strength MS medium. In the case of inhibitor treatments, plants were preincubated in the same medium with the indicated concentrations of inhibitors for 30 min before the FM4-64 pulse. In the case of salt stress experiments, plants were initially incubated in half-strength MS medium with or without the inhibitors for 15 min followed by supplementation with 100 mM NaCl and incubation for 30 min, prior to the addition of FM4-64. After the FM pulse, plants were fixed with 2% paraformaldehyde and imaged. For the quantification of FM4-64 uptake, average pixel intensity of the intracellular side of a cell excluding the PM and average pixel intensity of the PM were measured with ImageJ software (http://rsb.info.nih.gov/ij/), and the ratio of intensities between the intracellular area and the PM was calculated as a measure of dye uptake. The experiments were repeated twice (unless mentioned otherwise) with at least 200 cells quantified per treatment per experiment. Average fluorescence intensity (intracellular/PM) was calculated for each image, which is considered as a single data point. For plotting the data, the weighted mean (μ) of such average intensities was calculated as described before (Varma and Mayor, 1998) using the following formula:

$$\mu = \frac{\sum\left(\frac{n_i \mu_i}{\sigma_i^2}\right)}{\sum\left(\frac{n_i}{\sigma_i^2}\right)} \quad (1)$$

where n_i is the number of images quantified, μ_i is the mean, and σ_i is the SD of single data points (fluorescence intensity values of single images) in the *i*th experiment.

The deviation of the mean between experiments (σ_{mean}) was used to plot the error bars calculated using the following formula:

$$\sigma_{mean} = \sqrt{\frac{\sum (\mu - \mu_i)^2}{N}} \quad (2)$$

where N is the total number of experiments. Statistical significance was measured using an unpaired, two-tailed Student's *t* test. The quantification and measurement of LTI6b-GFP uptake were done in similar way.

Size Estimation of BFA Bodies and Vacuoles

The average surface area (in square pixels) of GFP-GPI- or FM4-64-containing BFA bodies in epidermal cells of Arabidopsis roots treated either with BFA or NAA/BFA was measured using ImageJ software. The plotted data are averages of three independent experiments with a minimum of 150 BFA bodies quantified per treatment per experiment.

For the measurement of vacuolar area in stele cells, the total surface area of vacuolar structures in a cell (in square pixels) at the median plane was measured and divided by the surface area of the cell at that plane. The data were plotted as a percentage of cellular area occupied by vacuoles. Plotted data are sums of two independent experiments with at least 100 cells quantified per genotype per condition (control or 100 mM NaCl). Weighted means and errors were calculated using Equations 1 and 2, respectively. Statistical significance was measured using an unpaired, two-tailed Student's *t* test.

Quantification of the Number of VPS9a-GFP Intracellular Punctae

To quantify the number of intracellular punctate structures of VPS9a-GFP in control plants and salt-stressed plants, individual frames of cells imaged in midplane were analyzed using Fiji software. Each image was thresholded such that only punctate structures were visible. After converting the images to binary masks, the number of punctate structures was counted with an automatic particle detection tool. The minimum diameter for detecting a body was four pixels.

Measurement of Root Growth Inhibition by Salinity and Drought

For measurement of the inhibition of root growth, 4-d-old wild-type and *vps9a-2* plants were transferred to solid half-strength MS medium, half-strength MS medium infused with 400 mg/mL PEG 6000 (Fluka) for drought stress, or half-strength MS medium with 100 mM NaCl for saline stress and grown vertically. The initial root length (*L*) and, after 10 d of growth, the increase in root length (ΔL) were measured for each plant. The percentage of inhibition (*I*) in root growth in response to salt stress in wild-type and *vps9a-2* plants was calculated as follows:

$$I = \left[1 - \left\{(\Delta L/L)_{stress}/(\Delta L/L)_{Control}\right\}\right] \; X \; 100 \qquad (3)$$

where ($\Delta L/L$) is the average value for a given condition (control or drought or salt) and genotype. The SE of ($\Delta L/L$) was used to plot the error bars.

Accession Numbers

Sequence data from this article can be found in the Arabidopsis Genome Initiative or GenBank/EMBL databases under the following accession numbers: VPS9a (At3g19770), ARA7 (At4g19640), ARA6 (At3g54840), CLC (At2g20760), COBRA (At5g60920), SKU5 (At4g12420), PIN2 (At5g57090), PIN1 (At1g73590), LTI6b (At3g05890), SMT2 (At1g20330), SMT3 (At1g76090), and SYP22 (AT5g46860).

Supplemental Data

Supplemental Figure 1. Subcellular localization of GPI-anchored proteins.

Supplemental Figure 2. Trafficking properties of endogenous GPI-anchored protein SKU5-GFP.

Supplemental Figure 3. VAEM imaging of CLC-GFP and mCherry-GPI foci on the plasma membrane.

Supplemental Figure 4. Effect of NAA on clathrin-dependent endocytosis.

Supplemental Figure 5. Effect of NAA on LTI6b-GFP and FM4-64 uptake.

Supplemental Figure 6. NAA blocks endocytosis in stele cells.

Supplemental Figure 7. Endocytosis in the presence of Tyr-A23.

Supplemental Figure 8. Salt-induced bulk flow pathway in Arabidopsis roots.

Supplemental Figure 9. Salt-induced increase of plasma membrane sterol content of internal cells.

Supplemental Figure 10. Salt sensitivity associated with sterol biosynthetic defects.

Supplemental Figure 11. Association of VPS9a-GFP with plasma membrane under salt stress.

Supplemental Figure 12. Expansion of vacuolar structures in stele in response to salt stress.

Supplemental Movie 1. Time-lapse VAEM imaging of root epidermal cell expressing CLC-GFP and mCherry-GPI.

Supplemental Movie 2. Clathrin-dependent uptake of mCherry-GPI.

Supplemental Movie 3. Clathrin-independent uptake of mCherry-GPI.

Supplemental Movie 4. Z-stack imaging of GFP-GPI Arabidopsis root treated with 10 μM NAA for 30 min and then 10 μM NAA + 50 μM BFA for 60 min.

Supplemental Movie 5. Z-stack imaging of GFP-GPI Arabidopsis root treated with 50 μM BFA for 60 min.

Supplemental Methods 1.

ACKNOWLEDGMENTS

We thank Sebastian Bednarek, Francine Carland, Jiri Friml, Eva Benkova, Tsuyoshi Nakagawa, and John Sedbrook for sharing published materials. We thank Kalika Prasad and Utpal Nath for published material, use of the plant growth facility, critical reading of the article, and valuable input; Takashi Ueda and Tomohiro Uemura for published material and useful suggestions; Mariko Sunada, Kazuo Ebine, Emi Ito, and Ashvini Kumar Dubey for help with experiments; Pushkar Paranjpe for help with data analysis; Chitra Pattabiraman for critical reading of the article; and the CIFF facility of the National Centre for Biological Sciences for imaging infrastructure. This work was funded by internal grants from the National Centre for Biological Sciences-TIFR, by a National Centre for Biological Sciences fellowship, CSIR-JRF fellowship, and Bristol-Myers Squibb travel award to A.B., and by a JC Bose fellowship from the Government of India to S.M.

AUTHOR CONTRIBUTIONS

S.M., M.K.M., and A.B. designed the research. S.M. and M.K.M. guided the research. N.G.I. cloned the GFP-GPI cassette and generated GFP-GPI-expressing BY-2 cells and Arabidopsis plants. M.F. and A.N. provided the VAEM imaging setup and valuable plant lines, guided the VAEM experiments, and helped with writing. A.B. performed the experiments and analyzed the data. A.B., S.M., and M.K.M. wrote the article.

Received February 18, 2015; revised March 27, 2015; accepted April 10, 2015; published April 21, 2015.

REFERENCES

Andrews, R., and Ahringer, J. (2007). Asymmetry of early endosome distribution in *C. elegans* embryos. PLoS ONE **2:** e493.

Anil, V.S., Krishnamurthy, H., and Mathew, M.K. (2007). Limiting cytosolic Na^+ confers salt tolerance to rice cells in culture: A two-photon microscopy study of SBFI-loaded cells. Physiol. Plant. **129:** 607–621.

Apse, M.P., Aharon, G.S., Snedden, W.A., and Blumwald, E. (1999). Salt tolerance conferred by overexpression of a vacuolar Na^+/H^+ antiport in Arabidopsis. Science **285:** 1256–1258.

Bandmann, V., Müller, J.D., Köhler, T., and Homann, U. (2012). Uptake of fluorescent nano beads into BY2-cells involves clathrin-dependent and clathrin-independent endocytosis. FEBS Lett. **586:** 3626–3632.

Benková, E., Michniewicz, M., Sauer, M., Teichmann, T., Seifertová, D., Jürgens, G., and Friml, J. (2003). Local, efflux-dependent auxin gradients as a common module for plant organ formation. Cell **115:** 591–602.

Birnbaum, K., Shasha, D.E., Wang, J.Y., Jung, J.W., Lambert, G.M., Galbraith, D.W., and Benfey, P.N. (2003). A gene expression map of the Arabidopsis root. Science **302:** 1956–1960.

Blümer, J., Rey, J., Dehmelt, L., Mazel, T., Wu, Y.W., Bastiaens, P., Goody, R.S., and Itzen, A. (2013). RabGEFs are a major determinant for specific Rab membrane targeting. J. Cell Biol. **200:** 287–300.

Bolte, S., Talbot, C., Boutte, Y., Catrice, O., Read, N.D., and Satiat-Jeunemaitre, B. (2004). FM-dyes as experimental probes for dissecting vesicle trafficking in living plant cells. J. Microsc. **214:** 159–173.

Cabrera, M., and Ungermann, C. (2013). Guanine nucleotide exchange factors (GEFs) have a critical but not exclusive role in organelle localization of Rab GTPases. J. Biol. Chem. **288:** 28704–28712.

Carland, F., Fujioka, S., and Nelson, T. (2010). The sterol methyltransferases SMT1, SMT2, and SMT3 influence Arabidopsis development through nonbrassinosteroid products. Plant Physiol. **153:** 741–756.

Carland, F.M., Fujioka, S., Takatsuto, S., Yoshida, S., and Nelson, T. (2002). The identification of CVP1 reveals a role for sterols in vascular patterning. Plant Cell **14:** 2045–2058.

Chadda, R., Howes, M.T., Plowman, S.J., Hancock, J.F., Parton, R.G., and Mayor, S. (2007). Cholesterol-sensitive Cdc42 activation regulates actin polymerization for endocytosis via the GEEC pathway. Traffic **8:** 702–717.

Cutler, S.R., Ehrhardt, D.W., Griffitts, J.S., and Somerville, C.R. (2000). Random GFP:cDNA fusions enable visualization of subcellular structures in cells of Arabidopsis at a high frequency. Proc. Natl. Acad. Sci. USA **97:** 3718–3723.

Delcroix, J.D., Valletta, J.S., Wu, C., Hunt, S.J., Kowal, A.S., and Mobley, W.C. (2003). NGF signaling in sensory neurons: Evidence that early endosomes carry NGF retrograde signals. Neuron **39:** 69–84.

Dhonukshe, P., Aniento, F., Hwang, I., Robinson, D.G., Mravec, J., Stierhof, Y.D., and Friml, J. (2007). Clathrin-mediated constitutive endocytosis of PIN auxin efflux carriers in Arabidopsis. Curr. Biol. **17:** 520–527.

Dinneny, J.R., Long, T.A., Wang, J.Y., Jung, J.W., Mace, D., Pointer, S., Barron, C., Brady, S.M., Schiefelbein, J., and Benfey, P.N. (2008). Cell identity mediates the response of Arabidopsis roots to abiotic stress. Science **320:** 942–945.

Doherty, G.J., and McMahon, H.T. (2009). Mechanisms of endocytosis. Annu. Rev. Biochem. **78:** 857–902.

Ebine, K., et al. (2011). A membrane trafficking pathway regulated by the plant-specific RAB GTPase ARA6. Nat. Cell Biol. **13:** 853–859.

Eisenhaber, B., Wildpaner, M., Schultz, C.J., Borner, G.H., Dupree, P., and Eisenhaber, F. (2003). Glycosylphosphatidylinositol lipid anchoring of plant proteins. Sensitive prediction from sequence- and genome-wide studies for Arabidopsis and rice. Plant Physiol. **133:** 1691–1701.

Fujimoto, M., Arimura, S., Ueda, T., Takanashi, H., Hayashi, Y., Nakano, A., and Tsutsumi, N. (2010). Arabidopsis dynamin-related proteins DRP2B and DRP1A participate together in clathrin-coated vesicle formation during endocytosis. Proc. Natl. Acad. Sci. USA **107:** 6094–6099.

Galvan-Ampudia, C.S., Julkowska, M.M., Darwish, E., Gandullo, J., Korver, R.A., Brunoud, G., Haring, M.A., Munnik, T., Vernoux, T., and Testerink, C. (2013). Halotropism is a response of plant roots to avoid a saline environment. Curr. Biol. **23:** 2044–2050.

Geldner, N., Dénervaud-Tendon, V., Hyman, D.L., Mayer, U., Stierhof, Y.D., and Chory, J. (2009). Rapid, combinatorial analysis of membrane compartments in intact plants with a multicolor marker set. Plant J. **59:** 169–178.

Geldner, N., Friml, J., Stierhof, Y.D., Jürgens, G., and Palme, K. (2001). Auxin transport inhibitors block PIN1 cycling and vesicle trafficking. Nature **413:** 425–428.

Goh, T., Uchida, W., Arakawa, S., Ito, E., Dainobu, T., Ebine, K., Takeuchi, M., Sato, K., Ueda, T., and Nakano, A. (2007). VPS9a, the common activator for two distinct types of Rab5 GTPases, is essential for the development of *Arabidopsis thaliana*. Plant Cell **19:** 3504–3515.

Golani, Y., Kaye, Y., Gilhar, O., Ercetin, M., Gillaspy, G., and Levine, A. (2013). Inositol polyphosphate phosphatidylinositol 5-phosphatase9 (At5ptase9) controls plant salt tolerance by regulating endocytosis. Mol. Plant **6:** 1781–1794.

Grebe, M., Xu, J., Möbius, W., Ueda, T., Nakano, A., Geuze, H.J., Rook, M.B., and Scheres, B. (2003). Arabidopsis sterol endocytosis involves actin-mediated trafficking via ARA6-positive early endosomes. Curr. Biol. **13:** 1378–1387.

Hamaji, K., et al. (2009). Dynamic aspects of ion accumulation by vesicle traffic under salt stress in Arabidopsis. Plant Cell Physiol. **50:** 2023–2033.

He, J.X., Fujioka, S., Li, T.C., Kang, S.G., Seto, H., Takatsuto, S., Yoshida, S., and Jang, J.C. (2003). Sterols regulate development and gene expression in Arabidopsis. Plant Physiol. **131:** 1258–1269.

Inoue, T., Kondo, Y., Naramoto, S., Nakano, A., and Ueda, T. (2013). RAB5 activation is required for multiple steps in *Arabidopsis thaliana* root development. Plant Cell Physiol. **54:** 1648–1659.

Kim, S.J., and Bassham, D.C. (2011). TNO1 is involved in salt tolerance and vacuolar trafficking in Arabidopsis. Plant Physiol. **156:** 514–526.

Kitakura, S., Vanneste, S., Robert, S., Löfke, C., Teichmann, T., Tanaka, H., and Friml, J. (2011). Clathrin mediates endocytosis and polar distribution of PIN auxin transporters in *Arabidopsis*. Plant Cell **23:** 1920–1931.

Kleine-Vehn, J., Leitner, J., Zwiewka, M., Sauer, M., Abas, L., Luschnig, C., and Friml, J. (2008). Differential degradation of PIN2 auxin efflux carrier by retromer-dependent vacuolar targeting. Proc. Natl. Acad. Sci. USA **105:** 17812–17817.

Konopka, C.A., and Bednarek, S.Y. (2008). Variable-angle epifluorescence microscopy: A new way to look at protein dynamics in the plant cell cortex. Plant J. **53:** 186–196.

Konopka, C.A., Backues, S.K., and Bednarek, S.Y. (2008). Dynamics of *Arabidopsis* dynamin-related protein 1C and a clathrin light chain at the plasma membrane. Plant Cell **20:** 1363–1380.

Kotzer, A.M., Brandizzi, F., Neumann, U., Paris, N., Moore, I., and Hawes, C. (2004). AtRabF2b (Ara7) acts on the vacuolar trafficking pathway in tobacco leaf epidermal cells. J. Cell Sci. **117:** 6377–6389.

Kumari, S., and Mayor, S. (2008). ARF1 is directly involved in dynamin-independent endocytosis. Nat. Cell Biol. **10:** 30–41.

Langhorst, M.F., Reuter, A., Jaeger, F.A., Wippich, F.M., Luxenhofer, G., Plattner, H., and Stuermer, C.A. (2008). Trafficking of the microdomain scaffolding protein reggie-1/flotillin-2. Eur. J. Cell Biol. **87:** 211–226.

Laxmi, A., Pan, J., Morsy, M., and Chen, R. (2008). Light plays an essential role in intracellular distribution of auxin efflux carrier PIN2 in *Arabidopsis thaliana*. PLoS ONE **3:** e1510.

Leshem, Y., Melamed-Book, N., Cagnac, O., Ronen, G., Nishri, Y., Solomon, M., Cohen, G., and Levine, A. (2006). Suppression of Arabidopsis vesicle-SNARE expression inhibited fusion of H_2O_2-containing vesicles with tonoplast and increased salt tolerance. Proc. Natl. Acad. Sci. USA **103:** 18008–18013.

Leshem, Y., Seri, L., and Levine, A. (2007). Induction of phosphatidylinositol 3-kinase-mediated endocytosis by salt stress leads to intracellular production of reactive oxygen species and salt tolerance. Plant J. **51:** 185–197.

Li, Q., Lau, A., Morris, T.J., Guo, L., Fordyce, C.B., and Stanley, E.F. (2004). A syntaxin 1, Galpha(o), and N-type calcium channel complex at a presynaptic nerve terminal: Analysis by quantitative immunocolocalization. J. Neurosci. **24:** 4070–4081.

Li, R., Liu, P., Wan, Y., Chen, T., Wang, Q., Mettbach, U., Baluska, F., Samaj, J., Fang, X., Lucas, W.J., and Lin, J. (2012). A membrane microdomain-associated protein, *Arabidopsis* Flot1, is involved in a clathrin-independent endocytic pathway and is required for seedling development. Plant Cell **24:** 2105–2122.

Li, X., Wang, X., Yang, Y., Li, R., He, Q., Fang, X., Luu, D.T., Maurel, C., and Lin, J. (2011). Single-molecule analysis of PIP2;1 dynamics and partitioning reveals multiple modes of *Arabidopsis* plasma membrane aquaporin regulation. Plant Cell **23:** 3780–3797.

Luu, D.T., Martinière, A., Sorieul, M., Runions, J., and Maurel, C. (2012). Fluorescence recovery after photobleaching reveals high cycling dynamics of plasma membrane aquaporins in Arabidopsis roots under salt stress. Plant J. **69:** 894–905.

Mateus, A.M., Gorfinkiel, N., Schamberg, S., and Martinez Arias, A. (2011). Endocytic and recycling endosomes modulate cell shape changes and tissue behaviour during morphogenesis in Drosophila. PLoS ONE **6:** e18729.

Mayor, S., Parton, R.G., and Donaldson, J.G. (2014). Clathrin-independent pathways of endocytosis. Cold Spring Harb. Perspect. Biol. **6:** a016758.

Mazel, A., Leshem, Y., Tiwari, B.S., and Levine, A. (2004). Induction of salt and osmotic stress tolerance by overexpression of an intracellular vesicle trafficking protein AtRab7 (AtRabG3e). Plant Physiol. **134:** 118–128.

Men, S., Boutté, Y., Ikeda, Y., Li, X., Palme, K., Stierhof, Y.D., Hartmann, M.A., Moritz, T., and Grebe, M. (2008). Sterol-dependent endocytosis mediates post-cytokinetic acquisition of PIN2 auxin efflux carrier polarity. Nat. Cell Biol. **10:** 237–244.

Nelson, B.K., Cai, X., and Nebenführ, A. (2007). A multicolored set of in vivo organelle markers for co-localization studies in Arabidopsis and other plants. Plant J. **51:** 1126–1136.

Onelli, E., Prescianotto-Baschong, C., Caccianiga, M., and Moscatelli, A. (2008). Clathrin-dependent and independent endocytic pathways in tobacco protoplasts revealed by labelling with charged nanogold. J. Exp. Bot. **59:** 3051–3068.

Ortiz-Zapater, E., Soriano-Ortega, E., Marcote, M.J., Ortiz-Masiá, D., and Aniento, F. (2006). Trafficking of the human transferrin receptor in plant cells: Effects of tyrphostin A23 and brefeldin A. Plant J. **48:** 757–770.

Paciorek, T., Zazímalová, E., Ruthardt, N., Petrásek, J., Stierhof, Y.D., Kleine-Vehn, J., Morris, D.A., Emans, N., Jürgens, G., Geldner, N., and Friml, J. (2005). Auxin inhibits endocytosis and promotes its own efflux from cells. Nature **435:** 1251–1256.

Robert, S., et al. (2010). ABP1 mediates auxin inhibition of clathrin-dependent endocytosis in Arabidopsis. Cell **143:** 111–121.

Roche, Y., Gerbeau-Pissot, P., Buhot, B., Thomas, D., Bonneau, L., Gresti, J., Mongrand, S., Perrier-Cornet, J.M., and Simon-Plas, F. (2008). Depletion of phytosterols from the plant plasma membrane provides evidence for disruption of lipid rafts. FASEB J. **22:** 3980–3991.

Roudier, F., Fernandez, A.G., Fujita, M., Himmelspach, R., Borner, G.H., Schindelman, G., Song, S., Baskin, T.I., Dupree, P., Wasteneys, G.O., and Benfey, P.N. (2005). COBRA, an *Arabidopsis* extracellular glycosyl-phosphatidyl inositol-anchored protein, specifically controls highly anisotropic expansion through its involvement in cellulose microfibril orientation. Plant Cell **17:** 1749–1763.

Sabharanjak, S., Sharma, P., Parton, R.G., and Mayor, S. (2002). GPI-anchored proteins are delivered to recycling endosomes via a distinct cdc42-regulated, clathrin-independent pinocytic pathway. Dev. Cell **2:** 411–423.

Sauer, M., Paciorek, T., Benková, E., and Friml, J. (2006). Immunocytochemical techniques for whole-mount in situ protein localization in plants. Nat. Protoc. **1:** 98–103.

Sbalzarini, I.F., and Koumoutsakos, P. (2005). Feature point tracking and trajectory analysis for video imaging in cell biology. J. Struct. Biol. **151:** 182–195.

Scheres, B., Benfey, P., and Dolan, L. (2002). Root development. The Arabidopsis Book **1:** e101, doi/10.1199/tab.0101.

Sedbrook, J.C., Carroll, K.L., Hung, K.F., Masson, P.H., and Somerville, C.R. (2002). The *Arabidopsis* SKU5 gene encodes an extracellular glycosyl phosphatidylinositol-anchored glycoprotein involved in directional root growth. Plant Cell **14:** 1635–1648.

Smotrys, J.E., and Linder, M.E. (2004). Palmitoylation of intracellular signaling proteins: Regulation and function. Annu. Rev. Biochem. **73:** 559–587.

Takano, J., Miwa, K., Yuan, L., von Wirén, N., and Fujiwara, T. (2005). Endocytosis and degradation of BOR1, a boron transporter of *Arabidopsis thaliana*, regulated by boron availability. Proc. Natl. Acad. Sci. USA **102:** 12276–12281.

Tall, G.G., Barbieri, M.A., Stahl, P.D., and Horazdovsky, B.F. (2001). Ras-activated endocytosis is mediated by the Rab5 guanine nucleotide exchange activity of RIN1. Dev. Cell **1:** 73–82.

Taylor, M.J., Perrais, D., and Merrifield, C.J. (2011). A high precision survey of the molecular dynamics of mammalian clathrin-mediated endocytosis. PLoS Biol. **9:** e1000604.

Ueda, T., Yamaguchi, M., Uchimiya, H., and Nakano, A. (2001). Ara6, a plant-unique novel type Rab GTPase, functions in the endocytic pathway of *Arabidopsis thaliana*. EMBO J. **20:** 4730–4741.

Uemura, T., Ueda, T., Ohniwa, R.L., Nakano, A., Takeyasu, K., and Sato, M.H. (2004). Systematic analysis of SNARE molecules in Arabidopsis: Dissection of the post-Golgi network in plant cells. Cell Struct. Funct. **29:** 49–65.

Varma, R., and Mayor, S. (1998). GPI-anchored proteins are organized in submicron domains at the cell surface. Nature **394:** 798–801.

Verslues, P.E., Agarwal, M., Katiyar-Agarwal, S., Zhu, J., and Zhu, J.K. (2006). Methods and concepts in quantifying resistance to drought, salt and freezing, abiotic stresses that affect plant water status. Plant J. **45:** 523–539.

Viotti, C., et al. (2013). The endoplasmic reticulum is the main membrane source for biogenesis of the lytic vacuole in *Arabidopsis*. Plant Cell **25:** 3434–3449.

Wang, Q., Kong, L., Hao, H., Wang, X., Lin, J., Samaj, J., and Baluska, F. (2005). Effects of brefeldin A on pollen germination and tube growth. Antagonistic effects on endocytosis and secretion. Plant Physiol. **139:** 1692–1703.

Wang, Q., Zhao, Y., Luo, W., Li, R., He, Q., Fang, X., Michele, R.D., Ast, C., von Wirén, N., and Lin, J. (2013). Single-particle analysis reveals shutoff control of the Arabidopsis ammonium transporter AMT1;3 by clustering and internalization. Proc. Natl. Acad. Sci. USA **110:** 13204–13209.

Xu, J., and Scheres, B. (2005). Dissection of *Arabidopsis* ADP-RIBOSYLATION FACTOR 1 function in epidermal cell polarity. Plant Cell **17:** 525–536.